

Dense-fluid shear viscosity via nonequilibrium molecular dynamics*

W. T. Ashurst†

Sandia Laboratories, Livermore, California 94550

and

W. G. Hoover

Department of Applied Science, University of California at Davis, Davis, California 95616

and Lawrence Livermore Laboratory, Livermore, California 94550

(Received 24 September 1974)

A novel fluid-transport calculation by computer simulation, via nonequilibrium molecular dynamics, of laboratory methods of transport measurement is described. Shear viscosity of soft-sphere (r^{-12} potential) and Lennard-Jones particles ($r^{-12}-r^{-6}$ potential) has been obtained from molecular dynamic modeling of Couette flow. Soft-sphere deviations from Enskog theory are similar to those found for hard spheres by Alder, Gass, and Wainwright, using time-correlations of equilibrium molecular dynamic system fluctuations. For the Lennard-Jones shear viscosity near the triple-point region, there is agreement between the equilibrium calculation of Levesque, Verlet, and Kurkijarvi and the nonequilibrium results using 108 atoms in a cube. However, systems two and three cubes wide give lower results, which, when extrapolated with inverse width, yield close agreement with the experimental argon shear viscosity. Comparison of the Lennard-Jones shear viscosity with experimental argon data along the saturated vapor-pressure line of argon confirms our successful simulation of macroscopic viscous flow with few-particle nonequilibrium molecular dynamic systems. A new result of the nonequilibrium molecular dynamics is the characterization of *nonequilibrium distribution functions*, which might provide the basis for a perturbation theory of transport. Since momentum transport is primarily accomplished by the repulsive potential core for high temperatures, the Lennard-Jones shear viscosity must behave like the soft-sphere system for high temperatures [viscosity divided by (temperature) $^{2/3}$ is a function of density divided by (temperature) $^{1/4}$]. In fact, the calculated excess shear viscosity (that part above the zero-density temperature dependence) has been successfully correlated in terms of the 12th-power scaling variables for temperatures as low as the critical value (along the freezing line). The utilization of soft-sphere scaling variables yields relatively simple functions for describing both the excess shear viscosity and the thermal-conductivity behavior throughout the fluid phase. The introduction of these scaling variables also clearly reveals two features: (i) weak temperature dependence, and (ii) the sign of the temperature derivative at constant density (negative for shear viscosity and positive for thermal conductivity). While both of these features have been experimentally observed in simple fluid experimental data, their cause has not been previously traced to the dominance of the core potential. Thus, the soft-sphere scaling variables should be useful for correlating experimental data.

I. INTRODUCTION

Fluid transport of mass, momentum, and energy is proportional,¹ as a first approximation, to linear gradients of concentration, velocity, and temperature. Many fluids experimentally obey these linear relations and are known as Newtonian fluids. For dilute gases, where only isolated binary molecular collisions are important, the Boltzmann equation has excellent experimental agreement for the self-diffusion D , viscosity η , and thermal-conductivity λ transport coefficients.² For dense gases, where finite molecular size affects the collision frequency, Enskog's rigid-sphere transport model has been moderately successful.³ In addition to transport by molecular streaming motion, instant-

taneous transfers of momentum and energy between molecular centers occur in dense gases. Comparison of dense-gas transport data (temperature range 225–350°K) with Enskog-model estimates⁴ indicates an adequate portrayal for densities $N\sigma^3/V$ up to 0.2, which corresponds to 600 times atmospheric density for helium and only 160 times for argon. For liquid-argon shear viscosity, the model of Enskog predicts a uniform dependence upon density which is not observed experimentally. Therefore, to extrapolate transport properties beyond available data, or for very dense fluids, the alternative method of molecular dynamics offers the only realistic description of transport phenomena.

Molecular dynamics means the numerical solu-

tion of Newton's equations of motion. With the availability of electronic computers, solutions for as many as 1000 interacting particles are feasible.^{5,6} Equilibrium molecular dynamics has previously been used to calculate the average time correlation of fluctuations in equilibrium systems. Green, Kubo, and others⁷ have given explicit relationships for the transport coefficients in terms of these time correlations. Molecular dynamics studies of rigid-sphere transport by Alder, Gass, and Wainwright⁸ have revealed deviations from the Enskog model at high density. The exact rigid-sphere shear viscosity is about twice the Enskog value near the freezing density. This failure of the Enskog theory indicates that long-time many-body correlations, some decaying⁹ as $(\text{time})^{-3/2}$, are important in dense-fluid transport. However, a rigorous analytical treatment of the total correlations is not possible.

Many investigators have utilized the Green-Kubo relations combined with the Lennard-Jones intermolecular potential to describe transport in liquid argon. Rahman¹⁰ followed the motion of 864 atoms and calculated a self-diffusion coefficient within 15% of experimental values. Verlet¹¹ has presented similar results. Bruin¹² presented results for a 64-atom system for D , η , and λ at one density-temperature point near argon's critical point, and Lagar'kov and Sergeev¹³ presented D and η for two combinations of density-temperature (using 32 atoms). Comparison with experiment indicates disagreements of order 20%.

To obtain the transport coefficients directly, without using the Green-Kubo relations, we generate nonequilibrium systems with the desired flux by numerically simulating laboratory methods of transport measurement. The method is described in Sec. II and the results in Secs. III-V. Two advantages of this novel approach are (i) more efficient transport determination and (ii) the characterization of nonequilibrium velocity and spatial distribution functions. In this work we describe the successful simulation of Couette flow, which determines the shear viscosity coefficient.

II. MOLECULAR DYNAMICS

In most of this work we consider N (32 or 108) particles confined to a cube of volume V . The computer calculations have been carried out in reduced units. The reducing quantities are the molecular mass m , the kinetic energy kT_0 , where k is Boltzmann's constant and T_0 is the desired temperature, and the volume cube edge L ($=V^{1/3}$). Special boundaries on the z faces are used to produce nonequilibrium fluxes, and periodic x and y boundaries are used to reduce the influences of

finite size on the results. We have followed Verlet¹¹ in using the explicit time-centered finite-difference equation

$$\frac{\vec{r}_i(t + \Delta t) - 2\vec{r}_i(t) + \vec{r}_i(t - \Delta t)}{(\Delta t)^2} = \frac{\vec{F}_i}{m}(t) - O((\Delta t)^2)$$

for the particle accelerations. Notice that the particle velocities are not needed to follow particle trajectories. However, to define the time-dependent kinetic energy, a centered particle velocity is calculated as

$$\vec{v}_i(t) = (1/2\Delta t)[\Delta\vec{r}(t + \frac{1}{2}\Delta t) - \Delta\vec{r}(t - \frac{1}{2}\Delta t)],$$

where $\Delta\vec{r}(t \pm \frac{1}{2}\Delta t) = \vec{r}(t \pm \Delta t) - \vec{r}(t)$. Use of the two increments $\Delta\vec{r}$ reduces truncation errors relative to those resulting from differencing particle positions.

Various types of boundaries have been tried to simulate nonequilibrium flow. The simplest modification of a periodic system is a boundary condition that gives an impulse to atoms in the x direction as they cross a particular z plane, with the sign of the x impulse depending upon the sign of the z velocity component. Except at low density, we feel that this boundary condition would establish not a simple shear flow, but instead a roughly sinusoidal velocity profile. An additional complication is that, while energy is being dissipated throughout the system, no heat is being removed, and the system would heat up. Heating was encountered by Gosling, McDonald, and Singer¹⁴ in calculations using a somewhat different method, an applied sinusoidal external force which produced a sinusoidal velocity profile whose amplitude is inversely proportional to the shear viscosity coefficient.

With undirectional heat flow, periodicity in the flux direction is impossible. The thermal expansion required to maintain a uniform hydrostatic pressure implies a monotonic density variation in the flux direction. Thus we concluded that for systems free of external forces, nonperiodic boundaries would be needed to establish simple shear and heat flows.

The simplest nonperiodic boundary condition would force atoms reaching either z cube face to rebound with the z -face wall velocity component (the other two velocity components could be selected to maintain the overall energy or temperature). Such reflecting boundaries were very promising when first investigated for the soft-sphere system at low density. However, when the density was increased, this method produced a large density increase in the region near the wall (and a resulting decrease in the center), since the atoms repelled each other strongly but did not interact with the wall until they attempted to cross it. To

decrease the excess boundary density, moving walls with various repulsive potentials were tried, but nothing really very satisfactory was obtained. Consequently, the plane wall was replaced with a lattice layer translating at the desired velocity. The fixed solid-like arrangement of the wall atoms again imposed an unacceptable density gradient upon the system. Therefore, *fluid*-like walls were selected (even though more computation was required).

The fluid-wall system is shown in Fig. 1. A unit cube of fluid is driven by two fluid-wall regions at the z cube faces. Periodic x and y boundaries are used. The two fluid-wall regions are intended to provide realistic extensions of the bulk fluid with properties and gradients smoothly continuing into these regions. The smooth continuity into fluid-wall regions cannot be perfect, however, as the fluid particles never mix with the bulk fluid. The fluid-wall particles are confined in the z direction between the z cube face and a second plane chosen so that the fluid-wall density matches the bulk density. A typical plane is shown in Fig. 1. If any particle center attempts to cross any of the four bounding z planes, it is elastically reflected from that plane. This reflection is easily accomplished by checking each particle's new position and, if it has passed a z boundary, returning the particle to its previous position with a reversed velocity component. Thus a reflected particle behaves as if it had undergone an elastic collision at a distance half the current spatial increment from its previous position. Consequently, the bounding walls are somewhat fuzzy, with a width of order the average increment size.

External forces are applied *only* within the fluid-

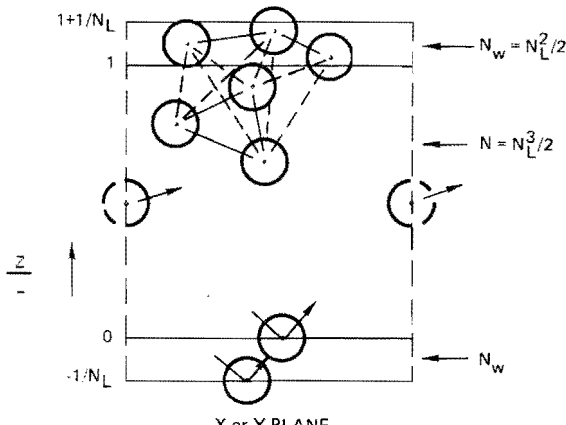


FIG. 1. Unit cube with N particles; N_w particles in each fluid-wall region maintain the desired z -direction flow. The z planes shown elastically reflect particle centers. Periodic boundaries are used in the x and y directions. A few particles are shown for the case $N = \frac{1}{2}N_L$.

wall regions to maintain the desired gradient in the z direction. The rate of work done by these external forces is the product of force times velocity. Thus, if the external force is equal for each fluid-wall particle, no work will result if the fluid-wall particles have zero mean velocity. To maintain a net shear flow, with nonzero $\langle du_x/dz \rangle$, the external x -direction force must do work each time step, since the x -direction mean velocity will generally be nonzero. Elastic boundary collisions in the z direction induce impulsive changes in the mean z velocity component. In order to reduce the amount of external work done (and hence the amount of cooling required to maintain constant energy), it is desirable to rezero the average z -direction momentum whenever an elastic wall collision occurs. For each fluid wall, the total momentum loss due to elastic wall collisions is divided by the number of fluid-wall particles and added to *all* the particles of that fluid wall.

Only the potential bonds between the fluid-wall particles and the bulk particles (i.e., those bonds crossing the z cube faces) need to be balanced by external forces. For Couette flow, the x component of these external forces is equivalent to the wall shear stress times the area of the xy plane. The time-dependent external force (for each fluid-wall) is

$$\vec{F}_{\text{ext}}(t) = \frac{1}{N_w} \sum_{i=1}^{N_w} \vec{F}_i(t).$$

This external force, which acts on fluid-wall particles only, maintains a constant average fluid-wall velocity (zero for heat flow) while the distribution of fluid-wall particle positions and velocities is unconstrained. The distribution of particle velocities about the mean velocity $\langle v \rangle$ defines the fluid-wall kinetic temperature,

$$\frac{3}{2}(N_w - 1)kT(t) = \frac{1}{2}m \sum_{i=1}^{N_w} [\vec{v}_i(t) - \langle \vec{v} \rangle]^2.$$

To maintain a constant wall temperature T_w each velocity component is scaled (by, at most, a few percent) each time step by

$$[\vec{v}_i(t) - \langle \vec{v} \rangle]_{\text{new}} = [T_w/T(t)]^{1/2} [\vec{v}_i(t) - \langle \vec{v} \rangle]_{\text{old}}.$$

This velocity scaling corresponds to external heat transfer from the fluid wall; the product of external force and group average fluid-wall displacement is the external work. For steady-state Couette flow, the work done is equal to the heat removed from the fluid-wall regions. The actual heat transfer is the change in kinetic energy of the fluid-wall particles. This is determined by computing the velocity at time t , prior to velocity scaling, and subtracting its square from the square

of the actual new scaled velocity at time t .

A similar calculation can be used to determine thermal conductivity. To maintain a steady-state heat flow the rate at which heat is added to the hot fluid-wall to maintain its temperature is the energy flux through the system times the xy area and must be equal to the rate at which heat is removed from the cold fluid-wall to maintain its lower temperature. The time-average energy flux and temperature gradient between the walls (z cube faces) determine the thermal conductivity coefficient.

For the shear flow, the velocity profile is determined by dividing the distance between the fluid-wall regions into a number of zones (e.g., ten) and averaging fluid momentum, energy, and number density in each zone. Initially, the N particles are uniformly distributed (face-centered cubic structure). Zero bulk velocity is achieved by alternating the direction of the x , y , and z thermal velocity v_t [$= (kT/m)^{1/2}$] components of particle-pairs. The average flow velocity component (x direction) is initially made to vary linearly in the z direction. Since the outer zones have a nonzero mean velocity in the x direction, a local-zone temperature is given by subtracting the mean velocity squared from the local-zone kinetic energy. The flow temperature can now be defined as the average of the zone temperatures $\langle T \rangle_z$. The steady-state local temperature distribution in shear flow may also be used to estimate the thermal-conductivity coefficient. The energy dissipated by the shearing action leaves the system via heat conduction to the fluid-wall particles. For equal wall temperatures, a parabolic temperature distribution must develop with the quadratic coefficient depending upon the shear viscosity η , square of the shear rate $u_{x,z}^2$ ($u_x \equiv \langle v_x \rangle$), and the thermal conductivity λ ,

$$T(z) = T(0) - (\eta/2\lambda) u_{x,z}^2 z^2,$$

where z is the distance from the plane of symmetry. The thermal-conductivity value may be determined by fitting a quadratic to the zone temperatures and using the calculated shear viscosity. Because of the quadratic shear-rate dependence, the higher shear rates produce less scatter in this thermal conductivity estimate. Reference 15 presents a FORTRAN computer program of the non-equilibrium molecular-dynamic method.

For actual calculations an intermolecular potential must be specified. A soft-sphere system [potential $\phi_{ss}(r) = \epsilon(s/r)^{12}$] was initially investigated for several reasons.

First, the popular Lennard-Jones 6-12 potential

$$\phi_{LJ}(r) = 4\epsilon[(\sigma/r)^{12} - (\sigma/r)^6],$$

which combines the inverse 12th-power repulsion with an inverse 6th-power attraction, has been successfully used to describe gas and solid equilibrium properties and dilute-gas transport properties. Thus, after initial development of the computer technique using the inverse 12th potential, simple addition of the 6th-power attraction will yield a Lennard-Jones system. (The equivalent reduced number densities are $N\sigma^3/V$ and $Ns^3/\sqrt{2}V$.)

Second, each inverse n th-power potential has special scaling properties.^{16,17} The dynamic evolution for different systems with identical scaled initial conditions [time and length scales from $(kT/m)^{1/2}$ and $(V/N)^{1/3}$] and with the same dimensionless value of $(Ns^3/V)(\epsilon/kT)^{3/n}$ will be identical. Also, the reduced viscosity $\eta s^2(m\epsilon)^{-1/2}$ and the thermal conductivity $\lambda s^2(m/\epsilon)^{1/2}/k$, when divided by $(kT/\epsilon)^{1/2+2/n}$, are functions of $(Ns^3/V)(\epsilon/kT)^{3/n}$ only, not density and temperature separately, throughout the fluid phase (there is no gas-liquid phase transition for these pure repulsive systems). At high temperatures repulsive forces dominate and the Lennard-Jones system must approach the scaling behavior of the inverse 12th-power potential. For moderate temperatures the attractive-power effect might be amenable to analytical treatment by utilizing the nonequilibrium distribution function for this scalable potential as the basis for a transport perturbation theory. Equilibrium perturbation theory has already proved successful,¹⁸ but a successful nonequilibrium perturbation theory has not yet been developed.

III. SOFT-SPHERE SHEAR VISCOSITY

A. Nonequilibrium molecular dynamic results

Both the shear viscosity and the thermal-conductivity coefficients have been calculated for dense soft-sphere [$\phi = \epsilon(s/r)^{12}$] fluids using the nonequilibrium molecular-dynamic technique. Shear viscosity has been determined by simulating Couette flow.¹⁹ The momentum flux P_{xz} between the walls (z direction) corresponds to minus the shear stress $\tau_{xz} = \tau_{zx} = \eta(u_{x,z} + u_{z,x})$. For this flow, the hydrodynamic velocity components u_y and u_z are zero, while u_x has a simple dependence upon the z coordinate. For small wall velocity, a linear velocity profile is generated in a Newtonian fluid. The velocity profile also has a very small (of order $u_{x,z}^2$) cubic term due to the temperature dependence of the shear viscosity coefficient.²⁰ The viscosity coefficient may be determined from the measured velocity gradient across the channel and the wall shear force per unit area from

$$P_{xz} = -\eta u_{x,z} \quad (\text{note } u_{z,x} = 0).$$

A soft-sphere system¹⁶ has been investigated at reduced densities between $\frac{1}{2}\rho_f$ and ρ_f , where ρ_f is the reduced freezing density [$Ns^3/\sqrt{2}V = 0.813 \times (kT/\epsilon)^{1/4}$]. The initial development of the non-equilibrium molecular-dynamic method used 32 soft spheres at a reduced density corresponding to $\frac{3}{4}$ the freezing density. After the fluid-wall method was decided upon, two other system sizes were investigated (cubes of 108 and 256 particles) to determine an optimum size in terms of computational time and calculational uncertainty. The same reduced unit velocity gradient $u_{x,z}L(m/kT)^{1/2}$ was used for each system size, and each system was followed for 8000 time steps with $\Delta t = 0.002L(m/kT)^{1/2}$. At equilibrium such systems maintain the total (energy)/ NkT constant in the first four digits. For particles with potential parameters appropriate for argon ($s = 3.5 \text{ \AA}$, $\epsilon/k = 120^\circ\text{K}$) and at room temperature, the calculated nondimensional time period corresponds to a real time period of only 10^{-11} sec. The computer time on the SLL CDC 6600 is about 14 orders of magnitude greater, 10 min, 1 h, and 4 h, for $N=32$, 108, and 256.

The velocity profiles resulting from the three calculations are shown in Fig. 2. The 108-particle profile is much smoother than the 32-particle results. Increasing the system size to 256 particles does not noticeably further improve the velocity profile. Therefore a procedure of using several runs with $N=108$ was selected as a good compromise between a *very-large-system* calculation or a smaller system observed for a *very long time*.

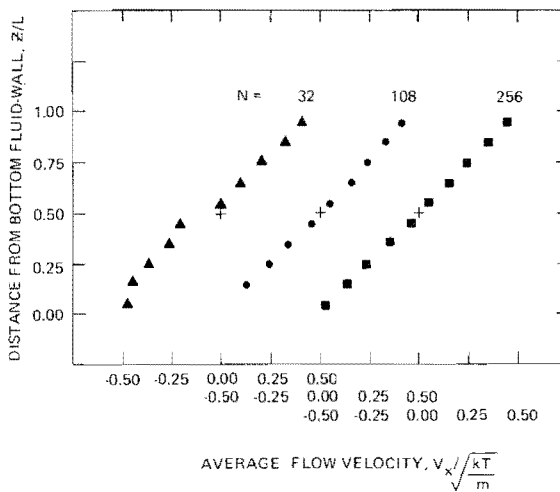


FIG. 2. Velocity profiles of soft-sphere Couette flow for three system sizes ($N=32$, 108, and 256) at $\frac{3}{4}$ freezing density. The reduced density [$Ns^3/(V\sqrt{2})](\epsilon/kT)^{1/4}$ is 0.576 with a reduced velocity gradient of $u_{x,z}L(m/kT)^{1/2} = 1$ and calculated with a reduced time step of 0.002 $\times L(m/kT)^{1/2}$ for 8000 time steps.

In order to determine possible number dependence, some $N=32$ calculations have been made. Comparison with the 108 results (Table I) reveals differences that are within the calculational uncertainties.

Using 108 soft spheres in a cube, the shear viscosity has been calculated for reduced densities [$\rho(\epsilon/kT)^{1/4}$] of 0.4, 0.6, 0.7, and 0.8. The results are presented in Table I and in Fig. 3 as a function of shear rate. For the lowest density con-

TABLE I. Soft-sphere shear viscosity from nonequilibrium molecular dynamics. Dependence on system size, shear rate, and density for the isotherm $\epsilon = kT$: $N = 32$ and 108 soft spheres in a cube with $N_w = 8$ and 18 soft spheres in each fluid wall (* indicates a two-layer fluid wall with $N_w = 36$). The $N = 216$ system is composed of two 108-particle cubes. A "run" includes 8000 time steps of $0.002L(m/kT_0)^{1/2}$, where L is the cube edge length and T_0 is the desired temperature. Beginning runs that reflected starting conditions were rejected. The shear rate $\omega = u_{x,z}$ and temperature T are averages over the 10 zones of bulk fluid. The shear viscosity η is calculated from the average wall shear stress and the averaged shear rate. Standard error is computed from the individual run values of the viscosity.

N	Runs used	$\frac{Ns^3}{\sqrt{2}V}$	$\omega s \left(\frac{m}{\epsilon} \right)^{1/2}$	$\frac{kT}{\epsilon}$	$\frac{\eta s^2}{(m\epsilon)^{1/2}}$
32	1-4	0.4	0.19	0.98	0.45 ± 0.03
	2-4		0.16	0.95	0.50 ± 0.01
	1-3		0.05	0.99	0.33 ± 0.1
32	1-4	0.6	0.29	0.97	1.37 ± 0.08
	1-4		0.22	0.99	1.26 ± 0.08
	1-6		0.15	1.00	1.30 ± 0.17
	1-4		0.08	1.01	1.18 ± 0.22
32	0.6 Estimate for zero shear rate				1.3 ± 0.1
	2-4	0.6	0.21	0.96	1.25 ± 0.04
	1-4		0.16	0.97	1.30 ± 0.02
	2-4		0.10	0.98	1.38 ± 0.04
	1-4		0.05	0.99	1.44 ± 0.1
108	0.6 Estimate for zero shear rate				1.5 ± 0.1
	2-7	0.7	0.16	1.01	2.34 ± 0.17
	1-4	0.7	0.11	0.98	2.27 ± 0.6
	1-4		0.05	0.99	2.54 ± 0.2
	0.7 Estimate for zero shear rate				2.8 ± 0.2
108	2-5	0.8	0.17	0.99	4.14 ± 0.12
	2-5		0.12	0.99	4.05 ± 0.13
	2-5		0.05	1.00	4.96 ± 0.6
	2-5*		0.05	1.00	5.7 ± 0.5
	0.8 Estimate for zero shear rate				5.4 ± 0.5
216	2-5	0.8	0.12	0.96	4.7 ± 0.1

sidered (0.4), the large-shear-rate result has the lower uncertainty and thus appears to provide the best estimate. For a reduced density of 0.6, shear rates of $u_{x,z} L(m/kT)^{1/2} = \frac{1}{4}, \frac{1}{2}, \frac{3}{4}$, and 1 with $N = 108$ produced a slight shear viscosity dependence upon shear rate; see Fig. 3. Comparison of 32-particle and 108-particle results indicates no difference larger than the calculational uncertainties. A linear extrapolation of the 108-particle results with shear rate yields a zero-shear-rate viscosity of $(1.5 \pm 0.1)(kT/\epsilon)^{2/3}(m\epsilon)^{1/2}/s^2$. Shear-rate dependence is larger for 0.7 reduced density, and linearly extrapolating the two calculated shear-rate values ($N=108$) yields $(2.8 \pm 0.2)(kT/\epsilon)^{2/3} \times (m\epsilon)^{1/2}/s^2$ (the 32-particle result at larger shear rate does not disagree with this extrapolation).

Near the freezing density, the shear-rate dependence becomes much larger. The shear viscosity at a reduced density of 0.8 was calculated at three shear rates, $u_{x,z} L(m/kT)^{1/2} = \frac{1}{4}, \frac{1}{2}$, and $\frac{3}{4}$. Fitting these results to the Ree-Eyring relation,²¹ $\eta/\eta_0 = (\sinh^{-1}\tau u_{x,z})/\tau u_{x,z}$, yields a zero-shear-rate viscosity of $\eta_0 = 5.0(kT/\epsilon)^{2/3}(m\epsilon)^{1/2}/s^2$, with a relaxation time of $\tau = 9.2 \text{ s}(m/\epsilon)^{1/2}(\epsilon/kT)^{7/12}$ (with a fit error of 8%). This relaxation time corresponds to 20 times the period of an Einstein oscillator in a face-centered crystal at the same density.

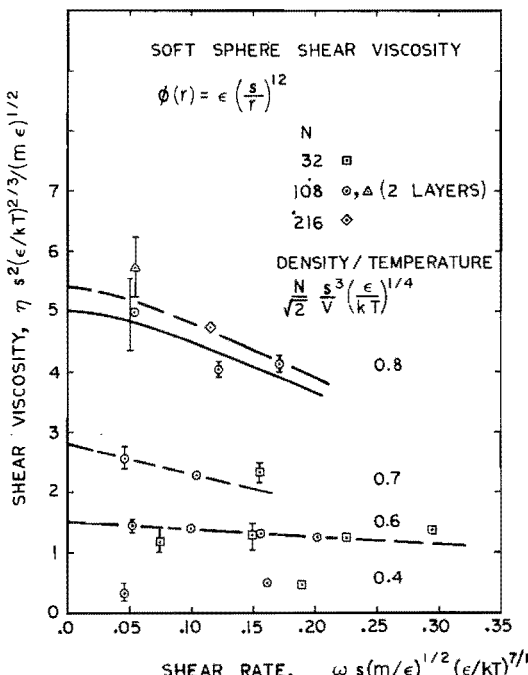


FIG. 3. Soft-sphere shear viscosity dependence upon shear rate and system size for the $\epsilon = kT$ isotherm at reduced densities $N(s/L)^3/\sqrt{2}$ of 0.4, 0.6, 0.7, and 0.8. Four-run viscosity averages are shown (vertical line denotes one standard error); a single run is 8000 time steps of $0.002 L(m/kT)^{1/2}$. See Table I.

The two-layer ($N_w = 36$) result at the lowest shear rate appears to have a larger viscosity value. Considering the standard errors, an average of the two means might be the best estimate. A fit of all four values with the \sinh^{-1} function yields 5.58, with a relaxation time of 13. Thus the zero-shear-rate viscosity is estimated to be $\eta s^2/(m\epsilon)^{1/2} \times (kT/\epsilon)^{2/3} = 5.4 \pm 0.5$. For the middle shear-rate value, the result for a system twice as wide (two 108 cubes together, $N = 216$) agrees with this estimate.

These zero-shear-rate shear-viscosity estimates are presented in Fig. 4 in terms of the 12th-power scaling variables,

$$\eta s^2(m\epsilon)^{-1/2}(\epsilon/kT)^{2/3}$$

versus

$$x \equiv [Ns^3/(\sqrt{2}V)](\epsilon/kT)^{1/4}.$$

The excess shear viscosity $\Delta\eta \equiv \eta - \eta_0$, where the dilute-gas limit is

$$\eta_0 s^2(m\epsilon)^{-1/2}(\epsilon/kT)^{2/3} = 0.171,$$

can be approximated (~10% error) by

$$\Delta\eta s^2(m\epsilon)^{-1/2}(\epsilon/kT)^{2/3} = 12.1x^4$$

(see Fig. 4). An equally good fit is obtained with the exponential function $e^{bx^4} - 1$, which is similar to Andrade's expression for liquid shear viscosity $Ae^{b/T}$. A better fit (~1% error) is given by the empirical relation

$$\Delta\eta s^2(m\epsilon)^{-1/2}(\epsilon/kT)^{2/3} = 0.022(e^{8.83x} - 1).$$

For density near zero, this fit indicates a first density correction of 0.15x, 10% larger than the Enskog value. Fitting with the density correction

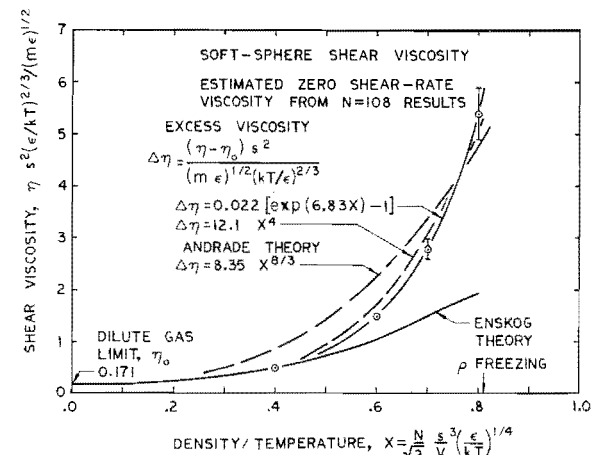


FIG. 4. Estimated zero-shear-rate infinite-system soft-sphere shear viscosity versus (reduced density)/(temperature)^{1/4}. This curve provides the complete fluid-phase shear-viscosity variation.

constrained to the Enskog value ($0.13x$) yields coefficients of 0.0191 and 7.02 and changes the curve very little.

B. Approximate models

The best-known approximate model for dense-fluid transport is Enskog's treatment of hard spheres which estimates the instantaneous transport of momentum and energy when two spheres collide.¹ The transport coefficients depend upon the collision frequency, which for hard spheres is related to the equation of state $y = PV/NkT - 1$. The Enskog model for hard-sphere transport can be applied to the soft-sphere system by determining y from the thermal pressure,

$$y = \frac{V}{NkT} T \left(\frac{\partial P}{\partial T} \right)_v - 1,$$

and the effective hard-sphere second virial coefficient (b) from

$$b = B + T \frac{dB}{dT},$$

where $B(T)$ [$= 3.62959x$] is the soft-sphere second virial coefficient.^{1,16} The soft-sphere thermal pressure was determined from Hansen's fit of Monte Carlo equation-of-state results.^{16,22}

The Enskog shear viscosity and thermal conductivity compared to their dilute-gas values are

$$\eta_E/\eta_0 = b\rho(y^{-1} + 0.8 + 0.761y)$$

and

$$\lambda_E/\lambda_0 = b\rho(y^{-1} + 1.2 + 0.755y).$$

The first approximation to the dilute-gas thermal conductivity is

$$\lambda_0 s^2 k^{-1} (m/\epsilon)^{1/2} (\epsilon/kT)^{2/3} = 0.642.$$

The three terms in the Enskog expressions have been called the "kinetic," "cross," and "potential." The "kinetic" term and half the "cross" term represent (kinetic) transport by streaming motion and the "potential" term and half the "cross" term represent transport by (potential) collision trans-

fer. Table II presents both the Enskog shear viscosity and thermal-conductivity coefficients for the soft-sphere system. As the density is increased to freezing, the magnitude of the streaming motion remains almost constant, in contrast to the large change in the collisional transfer (the former has 20 and 70% increases for η and λ , while the latter increases from 0 to ~ 12 times the dilute-gas value). This is similar to the density behavior of equilibrium properties, where the kinetic contribution is independent of density.

The Enskog-model viscosity at a reduced density of 0.6 is

$$\eta s^2 (m\epsilon)^{-1/2} (\epsilon/kT)^{2/3} = 1.05,$$

while the molecular-dynamic value is 1.5, a ratio of exact to Enskog estimate of 1.4 ± 0.1 . Alder, Gass, and Wainwright⁸ found a 1.10 ± 0.04 ratio for hard-spheres at $\frac{3}{4}$ the freezing density. The freezing-density soft-sphere shear viscosity is approximately $2\frac{1}{2}$ to 3 times the Enskog value (Alder *et al.* found 2.16 ± 0.09 for hard spheres at freezing). Thus the soft-sphere deviations from Enskog theory are similar to (but a bit larger than) those found for hard spheres by Alder *et al.* The hard-sphere molecular-dynamic results were obtained by time correlation of equilibrium-system fluctuations.

A second approximate estimate for shear viscosity can be obtained from the simple, but surprisingly quantitative, paradigm of Andrade. Andrade suggested that the viscosity of a simple liquid near its freezing point can be estimated by considering a particle to oscillate at the solid-like frequency, transferring transverse momentum to its neighbors at each turning point. Assuming that $\frac{1}{3}$ of the particles travel in the shear momentum flux direction yields the simple relation²³

$$\eta = 4mv/3s.$$

Using the experimentally determined solid vibrational frequencies and Lindemann's melting rule, Andrade found quite good agreement with available experimental data (in 1934) for mercury, lead, tin, copper, and bismuth. Andrade's relation for

TABLE II. Enskog estimate for soft-sphere shear viscosity η_E and thermal conductivity λ_E based on the thermal pressure y .

$\frac{Ns^3}{\sqrt{2V}} \left(\frac{\epsilon}{kT} \right)^{1/4}$	$\frac{PV}{NkT}$	y	$\frac{\eta_E s^2}{(m\epsilon)^{1/2}} \left(\frac{\epsilon}{kT} \right)^{2/3}$	$\frac{\lambda_E s^2}{k(\epsilon/m)^{1/2}} \left(\frac{\epsilon}{kT} \right)^{2/3}$	$\frac{m\lambda_E}{k\eta_E}$	$\frac{m\lambda_E}{k\eta}$
0.0	1.0	0	0.17	0.64	3.75	
0.4	4.56	1.84	0.51	2.19	4.29	4.29
0.6	9.46	3.49	1.05	4.32	4.13	2.88
0.7	13.46	4.49	1.45	5.89	4.06	2.10
0.8	18.76	5.49	1.92	7.73	4.02	1.43

the melting-point viscosity (poise) becomes

$$\eta \frac{g}{\text{cm sec}} = 5.1 \times 10^{-4} (AT_m)^{1/2} V_A^{-2/3},$$

where A is the atomic weight, T_m is the melting temperature ($^{\circ}\text{K}$), and V_A is the solid-phase volume of a gram-atom (cm^3) at temperature T_m . For soft spheres the melting temperature is related to the density by

$$kT_m/\epsilon = (\rho_m/0.844)^4,$$

and thus the Andrade expression for the melting-point soft-sphere shear viscosity becomes

$$\eta s^2 (m\epsilon)^{-1/2} (\epsilon/kT)^{2/3} = 8.35 x_m^{8/3},$$

which does agree with the high-density soft-sphere molecular-dynamic results (and is about twice the Enskog estimate at the freezing density).

C. Relationship to other transport coefficients

Two dimensionless ratios that involve the shear viscosity with the other transport coefficients are the Prandtl ratio ($m\lambda/k\eta$) and the Stokes-Einstein ratio ($D\eta\sigma/kT$). Several simple liquids have a Prandtl ratio within 10% of 2.5. However, if k is replaced by specific heat (as in the usual form of the Prandtl number), then the ratios for argon (monatomic), nitrogen (diatomic), and carbon tetrachloride (polyatomic) differ much more.²⁴ The Enskog soft-sphere Prandtl ratio increases from the dilute gas value of 3.75 to a maximum of 4.33 at $y = 1.126$ ($x \approx 0.3$) and then slowly decreases to 4.02 at the freezing density ($x = 0.813$); see Table II. Using the Enskog soft-sphere thermal conductivity [the molecular dynamic results for hard and soft-sphere thermal conductivity indicate small deviations from the Enskog estimates (see Refs. 8 and 15)] with the nonequilibrium molecular-dynamic shear viscosity yields a Prandtl ratio that decreases with increasing density (for $x > 0.4$); see last column of Table II. The exact hard-sphere Prandtl ratio⁸ also decreases more than the Enskog value and at the freezing density is 1.89, and thus, like the soft-sphere results, is much closer to simple-liquid experimental values than is the Enskog estimate. Horrocks and McLaughlin²⁴ have suggested a thermal-conductivity paradigm similar in philosophy to Andrade's, which for the soft-sphere systems becomes

$$\lambda \frac{s^2}{k} \left(\frac{m}{\epsilon} \right)^{1/2} \left(\frac{\epsilon}{kT} \right)^{2/3} = 15.55 x^{8/3}.$$

Therefore these two approximations produce a constant Prandtl ratio of 1.86, in agreement with the molecular-dynamic hard-sphere freezing values; but independent of density and temperature.

The experimental simple-fluid Prandtl ratios indicate a *positive* temperature derivative, which the soft-sphere Prandtl ratio also exhibits. This is easily seen by considering the excess thermal conductivity and viscosity, which can be approximated by a single power of x (for liquid densities and temperatures the excess coefficients are essentially equal to the total coefficients). Thus a Prandtl ratio with a positive temperature derivative is produced if the power for $\Delta\eta$ is greater than that for $\Delta\lambda$. This is in fact the case, since the soft-sphere excess shear viscosity can be approximated by x^4 and the Enskog soft-sphere excess thermal conductivity by $x^{2.5}$.

The Stokes-Einstein formula relates the diffusion coefficient D of a macroscopic spherical body of diameter σ in a fluid with viscosity η to the fluid-sphere hydrodynamic condition

$$D\eta\sigma/kT = 1/c\pi,$$

where $c = 3$ if the viscous fluid sticks to the sphere surface, and $c = 2$ for a *slip* boundary.²⁵ It is interesting that *molecular* self-diffusion can be closely approximated by this hydrodynamic formula. Experimentally, D , η , and σ for liquid argon and sodium are in reasonable agreement with the Stokes-Einstein relation. Zwanzig and Bixon²⁶ have generalized the Stokes-Einstein relation to a sphere undergoing small oscillations at arbitrary frequency with arbitrary slip. Fourier inversion of the frequency-dependent relation yields qualitative agreement with molecular-dynamic velocity autocorrelation for the Lennard-Jones potential (simulation of liquid argon at 76°K). The hard-sphere results of Alder *et al.*⁸ are within 10% of the slip condition for densities down to $\frac{1}{3}$ of freezing. Of course, this relation will not be true for dilute gases since η becomes independent of density while self-diffusion becomes inversely proportional to density.

Equilibrium molecular dynamics was applied to several soft-sphere systems ($N=256$), and the self-diffusion coefficient was determined from the slope of the mean-square displacement by least-squares fitting of

$$\langle [\vec{r}(t+\tau) - \vec{r}(\tau)]^2 \rangle,$$

which approaches $6Dt$ for large t ; see Table III. The 256-particle results are in reasonable agreement with the 500-particle soft-sphere results of Ross and Schofield.²⁷ Both sets are a little higher than the smaller-system results ($N=32$ and 108) of Hiwatari *et al.*²⁸ The Enskog estimates for D are two or three times too large when the thermal pressure is used. Estimates using $y = PV/NkT - 1$ are closer to the molecular-dynamic results; see Table III. The ratio D/D_E resembles the behavior

of the hard-sphere system, but the soft-sphere ratio has *smaller* deviations from unity. The Enskog Stokes-Einstein value (see Table III) remains below the stick-wall condition (0.106), while the soft-sphere results are stick-like at low density, but the value increases with density and becomes slip-like at the freezing density (same as hard spheres). For reduced densities greater than 0.6, the soft-sphere molecular-dynamic results can be approximated by

$$\frac{D}{s} \left(\frac{m}{\epsilon} \right)^{1/2} \left(\frac{\epsilon}{kT} \right)^{5/12} = D_0 e^{-\alpha},$$

where $D_0 \approx 4.9$ and $c \approx 6.3$ and $\alpha \equiv \rho(\epsilon/kT)^{1/4}$. The experimental high-pressure (100–1000 atm) CO₂ results of Timmerhaus and Drickamer²⁹ also have the exponential form (with $D_0 \sim 15$, $c \sim 7.9$) and do not follow the Enskog model. Hiwatari *et al.* show that the soft-sphere and Lennard-Jones results agree better than do the Lennard-Jones and hard-sphere results. The experimental data for krypton can be described using the Lennard-Jones potential, and thus the soft-sphere scaling variables should be useful for correlating experimental data.

D. Shear flow pair distribution

This development of nonequilibrium molecular dynamics has provided exciting new results: the first proper evaluation of nonequilibrium pair distribution functions. For simple dense fluids the equilibrium pair distribution function $g(r)$ has been well characterized⁵ and utilized to calculate equilibrium fluid properties. The equilibrium pair distribution function is clearly spherically symmetric (no preferred direction), while^{30,31} the velocity gradient distorts the distribution, as a first approximation, into an ellipsoid with principle axes coinciding with those of the rate of strain tensor (two preferred directions—those of maximum and minimum shear-momentum flux). Sum-

ming the xz component of the microscopic-pressure tensor over the volume V yields the shear-momentum flux between the two walls bounding the Couette flow,

$$P_{xz}V = m \sum_{i=1}^N \dot{x}_i \dot{z}_i + \sum_{i \neq j}^N F(r_{ij}) \frac{x_{ij} z_{ij}}{r_{ij}}$$

The above expression is clearly symmetric in x and z . The first term corresponds to the dilute-gas kinetic streaming motion and is of little importance for dense-fluid transport. The second term is the potential contribution, which is zero for dilute gases. The term xz/r^2 can also be expressed as a spherical harmonic

$$(2\pi/15)^{1/2} (Y_2^1 - Y_2^{-1}).$$

Thus, if the nonequilibrium pair distribution function is expanded in spherical harmonics, only the xz/r^2 term will contribute to the shear viscosity coefficient. Following Pryde,³⁰ we express the shear-flow nonequilibrium pair distribution function as

$$g(\vec{r}) = g(r)[1 + (xz/r^2)\nu(r)u_{x,z}],$$

where $\nu(r)$ allows for a radial variation in the distortion induced by the velocity gradient and has units of time. To determine $\nu(r)$ in a nonequilibrium system, we need only average xz/r^2 . Figure 5 presents $g(r)$ and the product $g(r)\nu(r)$ for the soft-sphere system at about $\frac{3}{4}$ the freezing density. The potential part of the viscosity coefficient can be expressed

$$\eta_\phi = \frac{2\pi}{15} \left(\frac{N}{V} \right)^2 \int_0^\infty \frac{d\phi}{dr} g(r)\nu(r)r^3 dr.$$

The significant range of $\nu(r)$ is approximately two molecular diameters in the dense-fluid states we have studied.

Until now, little has been known about $\nu(r)$. Green³¹ replaced $\nu(r)$ by a constant value, which

TABLE III. Soft-sphere self-diffusion and Stokes-Einstein ratio from Enskog model and nonequilibrium molecular dynamics.

$\frac{Ns^3(\epsilon)}{\sqrt{2VkT}}^{1/4}$	$\frac{D}{s} \left(\frac{m}{\epsilon} \right)^{1/2} \left(\frac{\epsilon}{kT} \right)^{5/12}$	$\frac{D}{D_E}$	$\frac{D\eta_s}{kT}$
Estimate ^a	Soft-sphere ^b	Enskog	Soft-sphere
0.4	0.192	0.222	0.098
0.6	0.081	0.096	0.085
0.7	0.055	0.055	0.080
0.8	0.038	0.03 ^c	0.073

^a $D_E/D_0 = 1/Y$, where $Y = [(PV/NkT) - 1]/(\bar{b}\rho)$. Note: The thermal pressure is *not* used, and $D_0(m/\epsilon)^{1/2}(\epsilon/kT)^{5/12} = 0.251/x$.

^b From soft-sphere molecular dynamics with $N = 256$.

^c From Ross and Schofield, Ref. 27.

reproduces the exponential temperature-dependent shear viscosity experimentally found by Andrade,²³ Frenkel,³² and others.²³ Chapman³³ utilizes the concept of an integral formulation for shear viscosity to correlate the viscosity data of 22 liquid metals. It is possible to obtain an *approximate* functional form for $\nu(r)$ from equilibrium properties based on Stokes's assumption that the viscous stress $\eta u_{x,z}$ is equivalent to the elastic stress $G\gamma$ if the strain γ is replaced by strain rate times a phenomenological relaxation time τ_m so that $\tau_m = \eta/G$. If the fluid could be sheared without viscous flow, then the angle-averaged shear modulus for this supposed elastic medium would be (in the absence of thermal fluctuations)³⁴

$$\frac{GV}{NkT} = \frac{2\pi}{15} \frac{N}{kTV} \int_0^\infty g(r)(r^2\phi'' + 4r\phi')r^2 dr,$$

and integration by parts yields

$$\frac{GV}{NkT} = \frac{2\pi}{15} \frac{N}{kTV} \int_0^\infty \frac{d\phi}{dr} \frac{dg(r)}{d\ln r} r^3 dr.$$

By comparison with the previous equation for η_ϕ , we find

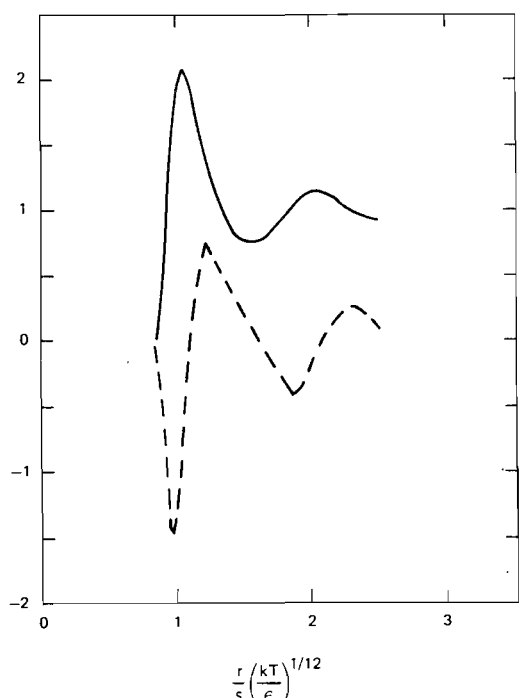


FIG. 5. Soft-sphere pair distribution for shear flow at $\frac{4}{3}$ freezing density $g(r)[1 + (xz/r^2)u_{x,z}\nu(r)]$. The spherically symmetric equilibrium term $g(r)$ is proportional to the probability of finding two particles a distance r apart (solid line). The total potential contribution to shear viscosity is given by the $\nu(r)$ term with xz/r^2 symmetry (dashed line). Calculated with $N=108$, $[N(s/L)^3/\sqrt{2}](\epsilon/kT)^{1/4}=0.576$, and $u_{x,z}L(m/kT)^{1/2}=1$.

$$\nu(r) \approx \tau_m \frac{d \ln g(r)}{d \ln r}.$$

Maxwell's relaxation time is $\tau_m \approx 10^{-13}$ sec for normal simple liquids. Therefore the nonequilibrium distribution function should be approximated by the change in the equilibrium distribution function caused by the applied strain. Figure 6 indicates this is a very good first approximation to the nonequilibrium distribution function. The elastic shear modulus G can be determined from the equilibrium hydrostatic pressure and internal energy. Zwanzig and Mountain have approximated G and τ_m from argon experimental data.³⁵ If the relaxation time could be determined from equilibrium properties or from a nonequilibrium reference system, then the shear viscosity would be known.

IV. LENNARD-JONES SHEAR VISCOSITY RESULTS

We first investigated the Lennard-Jones system along the saturated-vapor-pressure line and the freezing line. The excellent agreement with experimental argon data was very encouraging. About this time (January, 1973) Levesque, Verlet,

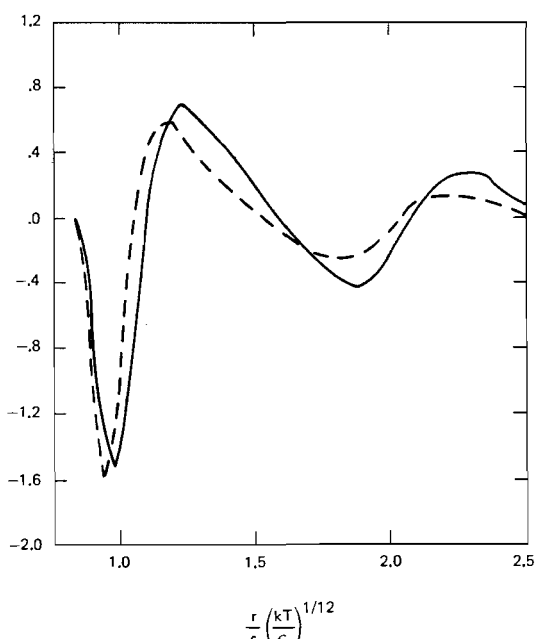


FIG. 6. Comparison of measured nonequilibrium part of the soft-sphere shear-flow pair distribution $[g(r)\nu(r)/L(m/kT)^{1/2}]$ with that obtained from the equilibrium distribution $[-\tau_m r d g(r)/dr]$ by applying a rate-of-shear displacement for a duration equal to Maxwell's relaxation time $\tau_m N^{1/3}/L(m/kT)^{1/2}=0.0991$. Conditions of Fig. 5, except a four-run average is shown. Integrating the non-equilibrium curve yields a potential shear viscosity of $\eta s^2/(m\epsilon)^{1/2}=1.18$, while the approximate curve (dashed) yields 1.23.

and Kurkijarvi sent us a report of work prior to publication describing their equilibrium molecular-dynamic calculation.³⁶ With some disappointment, we noted that our nonequilibrium molecular-dynamic viscosity near the triple point was some 25% below their equilibrium value for the Lennard-Jones shear viscosity. Comparison of the argon thermal conductivity with the results of the two molecular-dynamic methods revealed a similar disparity. The equilibrium molecular-dynamic thermal-conductivity coefficient is about twice the nonequilibrium molecular-dynamic and experimental argon values.

While the nonequilibrium results were closer to the experimental argon value, it must be remembered that the Lennard-Jones pair potential is only an approximation to argon.³⁷ The proper comparison is between the two different statistical methods of determining the Lennard-Jones shear viscosity coefficient. This discrepancy between the equilibrium and nonequilibrium results for the Lennard-Jones system could be due to number, boundary, or gradient dependence of the computer results, or to errors in the Green-Kubo formulation.

Preliminary runs were made to investigate the dependence of the nonequilibrium results upon velocity gradient and system size. For comparison with argon, a physically realistic extrapolation to macroscopic size should be used. The desired Newtonian shear viscosity coefficient is defined to be independent of the velocity gradient, but will depend upon whether the flow is laminar or turbulent. For Couette flow a laminar flow is expected¹⁹ for Reynolds numbers $Rn = (mpuL/\eta)$ below some critical value (~ 1500). The Reynolds number for our simulated Couette flow is of order one, and therefore our flow may safely be considered laminar. Any extrapolation to increased system size should maintain this laminar flow. If the velocity gradient were fixed, the Reynolds number would increase with system size as $Rn \sim L^2$, while, if the relative wall velocity difference is fixed, then $Rn \sim L$. In either case, a transition to turbulent flow would occur as L increases in size (although at a size *much* beyond current computation capabilities). Therefore, before number dependence can be determined, extrapolation to zero velocity gradient must be done, $Rn \sim 0$. Repeating this procedure for each system size allows a proper extrapolation to the macroscopic laminar hydrodynamic limit. Another difficulty arises in the small-gradient calculations. The average shear stress becomes much smaller than natural pressure fluctuations. In this case the boundary effects might lead to discrepancies with hydrodynamics.

tion to macroscopic size should be used. The desired Newtonian shear viscosity coefficient is defined to be independent of the velocity gradient, but will depend upon whether the flow is laminar or turbulent. For Couette flow a laminar flow is expected¹⁹ for Reynolds numbers $Rn = (mpuL/\eta)$ below some critical value (~ 1500). The Reynolds number for our simulated Couette flow is of order one, and therefore our flow may safely be considered laminar. Any extrapolation to increased system size should maintain this laminar flow. If the velocity gradient were fixed, the Reynolds number would increase with system size as $Rn \sim L^2$, while, if the relative wall velocity difference is fixed, then $Rn \sim L$. In either case, a transition to turbulent flow would occur as L increases in size (although at a size *much* beyond current computation capabilities). Therefore, before number dependence can be determined, extrapolation to zero velocity gradient must be done, $Rn \sim 0$. Repeating this procedure for each system size allows a proper extrapolation to the macroscopic laminar hydrodynamic limit. Another difficulty arises in the small-gradient calculations. The average shear stress becomes much smaller than natural pressure fluctuations. In this case the boundary effects might lead to discrepancies with hydrodynamics.

TABLE IV. Nonequilibrium molecular-dynamic results for Lennard-Jones shear viscosity near the triple point ($N\sigma^3/V = 0.8442$, $kT_0/\epsilon = 0.722$). Shear-viscosity dependence upon shear rate ($\omega = u_{x,z}$) and system width (in L units). See Table I caption (for $N = 324$, 15 zones were used). Apparent shear viscosity η_a was adjusted to the temperature T_0 by $\delta\eta/\eta = -0.65\delta T/T$. Thermal conductivity estimated from the zone-temperature distribution [coefficient of z^2 is $-\eta k\omega^2/(2\lambda m)$]. The experimental argon value is 6.5 ± 0.26 , Ref. 39, and the nonequilibrium molecular-dynamic simulation of heat-flow result is 6.6 ± 0.4 , Ref. 15.

Runs	$\omega\sigma\left(\frac{m}{\epsilon}\right)^{1/2}$	$\eta_a\sigma^2$ $(m\epsilon)^{1/2}$	$\frac{kT}{\epsilon}$	$\frac{\eta\sigma^2}{(m\epsilon)^{1/2}}$	$\lambda\frac{\sigma^2}{k}\left(\frac{m}{\epsilon}\right)^{1/2}$
$N = 108$ (L cube)					
4-9	0.0371	3.72 ± 0.22	0.724	3.73	4.7
4-9	0.0737	3.54 ± 0.11	0.715	3.52	8.0
1-4 ⁺	0.0852	3.41 ± 0.09	0.713	3.38	3.6
4-9	0.113	3.28 ± 0.01	0.711	3.24	8.1
1-6	0.156	3.07 ± 0.04	0.699	3.01	8.8
1-6	0.248	2.85 ± 0.06	0.672	2.72	6.5
$N = 216$ (2 L wide)					
2-5	0.0399	3.38 ± 0.17	0.721	3.37	4.7
2-5	0.0825	3.25 ± 0.15	0.689	3.15	14.0
3-6 ⁺	0.0885	3.21 ± 0.09	0.699	3.14	5.3
1-4	0.112	3.08 ± 0.05	0.681	2.96	6.3
$N = 324$ (3 L wide)					
2-6	0.0200	3.23 ± 0.17	0.717	3.22	?
3-7	0.0416	3.16 ± 0.06	0.707	3.12	9.5
3-6	0.0872	3.04 ± 0.05	0.670	2.90	6.3

A. Lennard-Jones triple-point shear viscosity—comparison with Green-Kubo method

An extensive set of nonequilibrium shear-viscosity calculations has been made in the triple-point region for comparison with the equilibrium molecular-dynamic calculation by Levesque, Verlet, and Kurkijarvi (LVK).³⁶ In the equilibrium work 864 particles were used with reduced density $N\sigma^3/V$ of 0.8442 and reduced temperature kT/ϵ of 0.722, approximately the triple-point values for both the Lennard-Jones system³⁷ and argon (using $\sigma=3.405 \text{ \AA}$ and $\epsilon/k=119.8^\circ\text{K}$, the reduced conditions become 1.418 g/cm^3 and 86.5°K). The real-time duration of the calculations was (for argon) 10^{-9} sec . The shear viscosity calculated from the Green-Kubo relation was

$$\eta\sigma^2/(m\epsilon)^{1/2} = 4.02 \pm 0.29.$$

For comparison with argon the calculated value is 3.64 mP, while Boon's experimental argon value is 2.71 mP ($\pm 2\%$).³⁸ The calculated equilibrium thermal-conductivity coefficient is $\lambda\sigma^2(m/\epsilon)^{1/2}/k = 14.8$, which is about twice the experimental argon value 6.5 ± 0.26 .³⁹ Nonequilibrium molecular-dynamic simulation of heat-flow results (6.6 ± 0.4)¹⁵ agree with the argon value.

Using 108 atoms in a cube, the nonequilibrium results for shear viscosity at the triple-point region indicated dependence upon shear rate—i.e., non-Newtonian behavior.¹⁵ The apparent viscosities for five different shear rates (averaged over a time period corresponding to 10^{-9} sec for argon) are given in Table IV and shown in Fig. 7. The local average flow temperatures (kinetic energy with respect to the mean velocity) were determined in the zones used to define the velocity profile. For the higher shear rates, the average temperature was approximately 5% below the desired temperature. Therefore the calculated shear viscosity was adjusted to the desired temperature. The experimental argon shear-viscosity pressure and temperature dependence from Hellemans *et al.*⁴⁰ and the estimate $(\partial \ln P / \partial \ln T)_v = 30.4$ were used to estimate temperature dependence at constant density, with the result

$$\left(\frac{\delta\eta}{\eta}\right)_p = -0.65 \frac{\delta T}{T} \quad \text{for the triple-point region.}$$

Hence, a 5% temperature increase corresponds to a 3% decrease of the shear viscosity.

For fixed N the dependence of apparent viscosity η ($= -P_{xx}/u_{x,z}$) on strain rate can be described by the Eyring model of non-Newtonian viscous flow,

$$\eta = \eta_0 (\sinh^{-1} \tau \omega) / \tau \omega,$$

where η_0 is the zero shear rate or Newtonian vis-

cosity, τ is a relaxation time, and ω is the shear rate $u_{x,z}$. While Eyring's model cannot directly predict η_0 and τ from molecular properties, it has been shown that this model can adequately portray the experimental data for many high-viscosity fluids. The Ree-Eyring model contains two additional parameters (two additive \sinh^{-1} viscosities) and successfully describes grease over six decades of shear force and nine decades of shear rate.²¹ The non-Newtonian flow found here in a monatomic fluid at high shear rates corresponds to that found in laboratory experiments at low shear rates on more complicated molecules.

Fitting the adjusted viscosities at the three lowest shear rates with the \sinh^{-1} function produces a 108-particle zero-gradient viscosity of $\eta_0 = 3.82(m\epsilon)^{1/2}/\sigma^2$ and a relaxation time of $\tau = 10.4\sigma(m/\epsilon)^{1/2}$. Including the two higher shear-rate values reduces η_0 and τ to 3.71 and 8.30, indicated by the dashed line in Fig. 7. This relaxation time corresponds to approximately 13 times the period of an Einstein oscillator in a face-centered Lennard-Jones crystal at this same density, $1/\nu_E = 0.80\sigma(m/\epsilon)^{1/2}$. The extrapolated 108-particle viscosity appears to be consistent with the Green-Kubo result of LVK, but with both methods predicting substantially larger values than the experimental argon data.

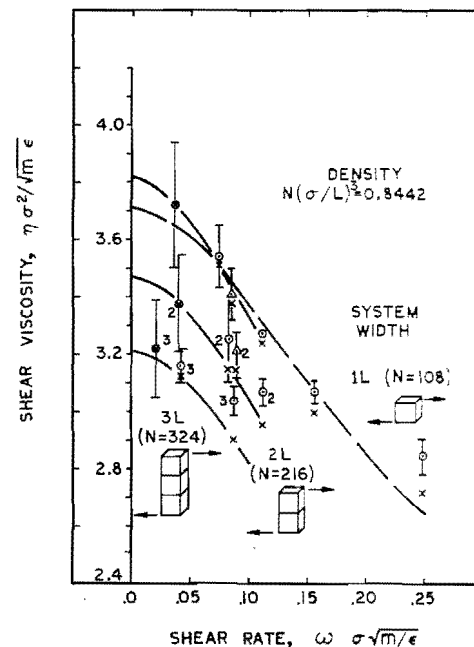


FIG. 7. Lennard-Jones shear viscosity dependence upon shear rate and system width at the triple-point region. Circles are the calculated mean values (vertical line denotes one standard error) and the 'x's are the estimated shear viscosity for $kT/\epsilon = 0.722$ (see Table IV).

The remaining extrapolation to macroscopic system size (while maintaining laminar flow conditions) was investigated by comparing the 108-particle viscosity with results from systems two and three 108 cubes wide. These larger-system results are also shown in Fig. 7 and Table IV. They are clearly lower than the 108-particle values. Fitting the 216-particle results with the \sinh^{-1} function produces a zero-gradient viscosity of $\eta_0 = 3.47(m\epsilon)^{1/2}/\sigma^2$ and a relaxation time of $\tau = 10.4\sigma(m/\epsilon)^{1/2}$. Thus doubling the system width decreases the zero-gradient viscosity value, while the relaxation time does not change. Assuming, in addition to gradient dependence, an inverse width dependence, so that η is a function of both ω and κ , leads to a hydrodynamic shear viscosity $\eta_{0,0}$ of $3.12(m\epsilon)^{1/2}/\sigma^2$. The uncertainty in this estimate is at least 5%.

To provide some confidence in this arbitrary extrapolation, a system three cubes wide ($N=324$) was studied at three shear rates. The mean values and temperature-adjusted values are also shown in Fig. 7, and again they are clearly lower than those found with smaller systems. The 324-particle results, fitted with the \sinh^{-1} function, produce a zero-gradient viscosity of $\eta_0 = 3.21(m\epsilon)^{1/2}/\sigma^2$ with a relaxation time of $10.0\sigma(m/\epsilon)^{1/2}$.

The mathematical similarity between stresses in viscous fluids and stresses in elastic solids⁴¹ can be used to support the inverse width dependence of the viscosity coefficient. Finite periodic harmonic crystals with fixed center of mass exhibit an elastic restoring force on a particle displaced a distance x from its equilibrium location. This force ($-\chi x$) is proportional to an elastic modulus, and the equilibrium mean-squared displacement is proportional to the reciprocal of the modulus,

$$F = -\chi x, \quad \langle x^2 \rangle = 3kT/\chi.$$

Numerical results given in Table V for harmonic crystals show that $\langle x^2 \rangle$ increases with system width,

$$\langle x^2 \rangle_N / \langle x^2 \rangle_\infty = 1 - c/N^{1/3},$$

where the constant c varies both with crystal structure and shape (Table V). Thus the elastic modulus (analogous to shear viscosity in a fluid) decreases with $1/N^{1/3}$ as the large-system limit is approached. For harmonic forces the viscosity dependence upon system width would be

$$\eta_N / \eta_\infty = 1 + c/N^{1/3},$$

where c is a constant of order 1, which is consistent with a curve fit of the nonequilibrium molecular-dynamic zero-gradient viscosity estimates. This same functional form is also in reasonable agreement with experimental hydrody-

namics. The wall correction for viscosity experiments in which a sphere of diameter σ is dropped in a tube of diameter D containing viscous liquid is $1 + (\sim 2)\sigma/D$, where the coefficient depends somewhat upon the cross-section shape.⁴²

The three parameters of interest ($\eta_{0,0}$, τ , and c —the coefficient of $1/N^{1/3}$) may also be determined by fitting all the temperature-adjusted shear viscosity with one general function,

$$\eta_{\omega,\kappa} = \eta_{0,0}(1 + ck)(\sinh^{-1}\tau\omega)/\tau\omega,$$

where $\eta_{\omega,\kappa}$ is the calculated shear-rate-dependent finite-width viscosity, $\eta_{0,0}$ is the zero shear-rate infinite-width viscosity, c is the coefficient for width dependence, and τ is the relaxation time for shear rate-dependence. Fitting the adjusted calculated shear viscosities of Table IV with the residuals weighted equally or by various functions of the width and/or calculated standard error produced a range of values for c (1.1–1.38) and τ (6.4–10.2), but little variation in the viscosity estimate,

$$\eta_{0,0} = 2.89(\pm 0.06)(m\epsilon)^{1/2}/\sigma^2.$$

Figure 8 presents the equal-weight fit along with the similarly adjusted Green-Kubo value ($c = 1.38$), and l is assumed to be half the cube edge, the largest possible separation of particles pairs in a periodic system; i.e., l is equal to the nonequilibrium 108-system width. Considering the uncertainties, it appears at present that the two molecular-dynamic methods (both adjusted to infinite width) agree with each other and with the experi-

TABLE V. Mean-squared displacement relative to the Einstein approximation, $3kT/4\chi_E$, where χ_E is the nearest-neighbor harmonic force constant, for N -particle harmonic crystals with nearest-neighbor interactions. These crystals are periodic with fixed center of mass. The large-crystal ratios are of the form R (fcc) = $1.679_4 - 1.56/N^{1/3}$ and R (hcp) = $1.668_5 - 1.16/N^{1/3}$.

N (fcc)	R (fcc)	N (hcp)	R (hcp)
4	0.833 333	2	1.500 000
32	1.220 430	16	1.344 141
108	1.361 392	54	1.402 399
256	1.437 691	128	1.451 938
500	1.484 843	250	1.488 476
864	1.516 722	432	1.515 363
1372	1.539 673	686	1.535 618
2048	1.556 973	1024	1.551 298
2916	1.570 474	1458	1.563 745
4000	1.581 300	2000	1.573 844
5324	1.590 173	2662	1.582 191
6912	1.597 578	3456	1.589 201
8788	1.603 849	4394	1.595 167
10976	1.609 623		
∞	1.6794	∞	1.6685

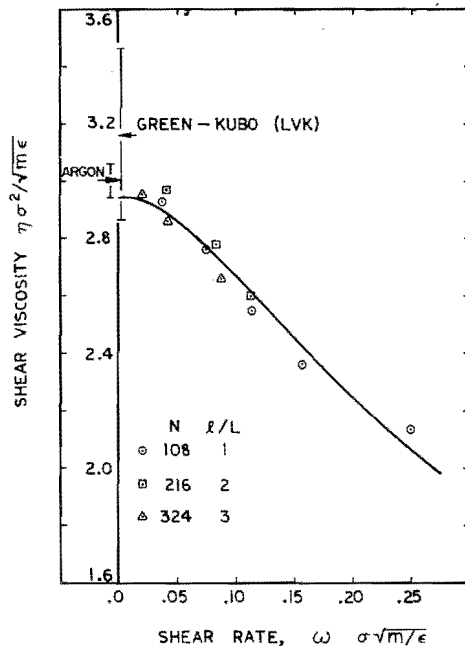


FIG. 8. Calculated Lennard-Jones shear viscosity at the triple-point region. The line is a nonlinear fit with a function having inverse hyperbolic sine shear-rate dependence and inverse width dependence. Also shown is the infinite-width-adjusted equilibrium (Green-Kubo) result of Levesque, Verlet, and Kurkijarvi and the experimental argon shear viscosity (with an estimated 2% uncertainty).

mental argon shear viscosity (also shown in Fig. 8 with the quoted 2% experimental error). Our final estimate for Newtonian shear flow near the Len-

TABLE VI. Nonequilibrium molecular-dynamic 108-particle results for Lennard-Jones shear viscosity along the argon saturated-vapor-pressure line (temperature and density in first two columns). Four-run average, see Table I caption ($N=324$); η_0 is the estimated zero-shear-rate viscosity, τ is the Eyring-Ree relaxation time, and η_E is the Enskog estimate.

nard-Jones triple-point region derived from the nonequilibrium molecular dynamics is $\eta\sigma^2/(m\epsilon)^{1/2} = 2.9(\pm 0.1)$. Therefore the apparent discrepancy between the two molecular-dynamic methods and the experimental argon data appears to be due to finite flow-field effects. This phenomenon is apparently confined to the triple-point region. Calculations with 108 and 324 systems at a reduced density of 0.76 on the svp line, and at 0.94 on the freezing line, indicate *no* significant width dependence.

B. Lennard-Jones shear viscosity along the saturated-vapor-pressure line

Hansen and Verlet³⁷ have found good agreement with experimental argon phase-diagram data using the Lennard-Jones pair-potential

$$\phi_L(r) = 4\epsilon [(\sigma/r)^{12} - (\sigma/r)^6],$$

with $\sigma = 3.405 \text{ \AA}$ and $\epsilon/k = 119.8^\circ\text{K}$. The melting-freezing agreement "confirms the excellence of the Lennard-Jones potential as an effective two-body potential for argon at high density." The agreement is not as good along the saturated-vapor-pressure line (especially near the critical temperature, $1.26 \epsilon/k$ for argon versus $1.36 \epsilon/k$ for Lennard-Jones). We calculated the Lennard-Jones shear viscosity along the experimental saturated-vapor-pressure line of argon; see Table VI. For argon, the real time durations are about 10^{-10} sec , while CDC 6600 computational time was approximately 10^4 sec .

It appears to be generally true that the lower-shear-rate results are somewhat (approximately 10%) larger. For the density of 0.85, the relaxation time and width correction determined from the extensive triple-point calculations was used. A one-constant fit of the two 108 results is $\eta_{0,0} = 3.29(m\epsilon)^{1/2}/\sigma^2$, which does agree with the experimental argon data. The inverse width correction is apparently only applicable to the very dense triple-point region. For a reduced density of 0.76 on the saturated-vapor line, the results of a 108-particle system and a 324-particle system indicate no significant width dependence. At the remaining two lower-density conditions, the calculated apparent shear viscosities for the two shear rates have error bars that overlap. Thus a two-constant fit is not really valid. However, the estimated zero-shear-rate viscosity values do not noticeably differ from the calculated low-shear-rate results.

Thermal pressures determined from the Lennard-Jones equation of state determined by Levesque and Verlet⁴³ have been used to make Enskog shear-viscosity estimates (shown in Table VI). For these densities and temperatures, the Enskog estimates lie approximately 20% below the molecular-dynamic results. For densities greater than critical and temperatures below critical, the Enskog estimates have similar disagreements with experimental data.⁴⁴

There is extensive experimental argon shear-viscosity data for comparison along the saturated-vapor-pressure line.^{38,40,45,46} Accuracy within a few percent is claimed for each set of experimental results. Yet the various methods of measuring the viscosity produce values differing by 10–50%. The recent experimental work by Haynes⁴⁶ using a torsional viscometer like DeBock *et al.*⁴⁵ indicates good agreement along the vapor-pressure line with the results of Hellemans *et al.*⁴⁰ (they used an oscillating disk viscometer). Away from the vapor-pressure line the pressure dependence of Haynes and DeBock *et al.* agree for the slope, but the latter work produced higher viscosity values. The results of Hellemans *et al.* indicated a much smaller pressure dependence, but their results away from the saturated liquid line are suspect since they used helium gas to pressurize the liquid argon and hence had a helium-argon mixture. The largest experimental differences occur for pressure-temperature values away from the vapor-pressure line and near the critical temperature. Some of the experimental differences may be due to uncertainty in the experimental pressure-temperature conditions.

Figure 9 compares the nonequilibrium molecular-dynamic estimates with the experimental

argon shear-viscosity data. Considering the disagreement among the experiments, it seems likely that the experimental and the calculated molecular-dynamic results have comparable uncertainties. The overall agreement indicates successful simulation of nonequilibrium shear flow with few-particle systems.

C. Lennard-Jones shear viscosity along the freezing line

The shear viscosity along the Lennard-Jones fluid freezing line has been calculated at temperatures up to four times the critical temperature. The results along with Enskog model shear-viscosity estimates are given in Table VII (thermal pressure from Hansen's high-temperature equation of state²²). These estimates are only 50% of the molecular-dynamic results, a discrepancy similar to that found by Alder, Gass, and Wainwright⁸ for hard spheres near their freezing density. The viscosity dependence on shear rate is shown in Fig. 10 together with a zero-shear-rate estimate (fitting the two-constant \sinh^{-1} function through the two calculated values). For a reduced density of 0.936, a 324-particle system agrees

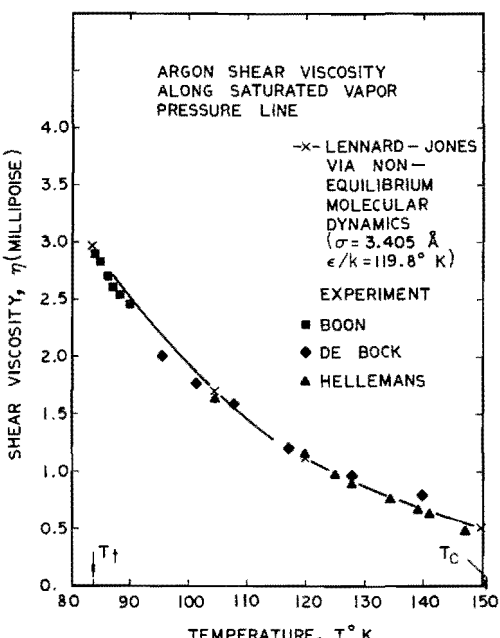


FIG. 9. Experimental argon shear-viscosity coefficient along saturated-vapor-pressure line. Boon *et al.* used a capillary viscometer with accuracy better than 3%; De Bock *et al.* used a torsionally vibrating piezoelectric quartz crystal; Hellemans *et al.* used an oscillating disk viscometer with accuracy better than 2%. The line is the estimated zero-shear-rate infinite-system-size Lennard-Jones shear viscosity from nonequilibrium molecular-dynamic calculations done with 108 atoms at two shear rates (see Table VI).

TABLE VII. Nonequilibrium molecular-dynamic 108-atom results for Lennard-Jones shear viscosity along the freezing line for temperatures (kT/ϵ) up to 5. Four-run average, see Table I caption (* $N=324$); η_0 is the estimated zero-shear-rate viscosity, τ is the Eyring-Ree relaxation time, and η_E is the Enskog estimate.

kT_0/ϵ	$N\sigma^3/V$	kT/ϵ	$u_{x,z}\sigma\left(\frac{m}{\epsilon}\right)^{1/2}$	$\frac{\eta\sigma^2}{(m\epsilon)^{1/2}}$	$\frac{\eta_0\sigma^2}{(m\epsilon)^{1/2}}$	$\frac{\tau\left(\frac{\epsilon^{1/2}}{m}\right)}{\sigma}$	$\frac{\eta_E\sigma^2}{(m\epsilon)^{1/2}}$
1.15	0.936	1.114	0.215	4.19 ± 0.09			
		1.132	0.104	4.63 ± 0.23			
		1.130	0.053	$4.79 \pm 0.18^*$			
2.0	1.04	1.955	0.305	5.65 ± 0.06		4.83	5.02
		1.976	0.145	6.36 ± 0.27			
2.74	1.113	2.668	0.364	6.79 ± 0.20		6.68	3.96
		2.740	0.171	7.76 ± 0.64			
5.0	1.279	4.857	0.521	10.51 ± 0.21		8.21	3.61
		4.954	0.250	10.95 ± 0.91			
						11.1	4.63
						1.16	

with the 108-particle results and thus indicates no width dependence. Therefore it is concluded that the width phenomenon only occurs for conditions very near the triple-point region.

It is interesting to note that the large-gradient viscosities have a linear dependence upon temperature, while the estimated zero-shear-rate viscosity values do not. The potential contribution to momentum transport is related to the elastic shear modulus (see Sec. III). Along the soft-sphere freezing line, this reduced shear modulus is a constant,

$$GV/NkT = 7.2 \langle \phi / NkT \rangle \approx 30.$$

Thus a rough estimate for the potential part of the shear viscosity is

$$\eta_\phi \sigma^2 (m\epsilon)^{-1/2} \approx 30 (\epsilon/m)^{1/2} (kT/\sigma\epsilon) \tau_m (N\sigma^3/V).$$

For the freezing-line conditions calculated, the temperature changes by a factor of 4.3 while the density only increases by 1.4. Therefore the linear temperature dependence at large shear rate appears reasonable. Of course, at high temperatures the repulsive core potential dominates momentum transport. Thus the high-temperature Lennard-Jones system must approach the behavior of the inverse-12th-power system. The special scaling feature leads to a simple relation for the soft-sphere shear viscosity along the freezing line,

$$[(\eta - \eta_0)\sigma^2/(m\epsilon)^{1/2}] (\epsilon/kT)^{2/3} = 4.1 (\pm 0.4).$$

A reasonable curve fit (~4% error) of the freezing-line Lennard-Jones reduced excess shear viscosity is

$$[(\eta - \eta_0)\sigma^2/(m\epsilon)^{1/2}] (\epsilon/kT)^{2/3} = 4 (\pm 0.15),$$

which does agree quite well with the soft-sphere result. A similar expression has been obtained by LVK.³⁶ Upon replacing the L-J molecules with hard spheres of diameter d (chosen to reproduce the equilibrium structure factor) and using the hard-sphere viscosity results of Alder *et al.* along with the low-temperature L-J freezing-temperature

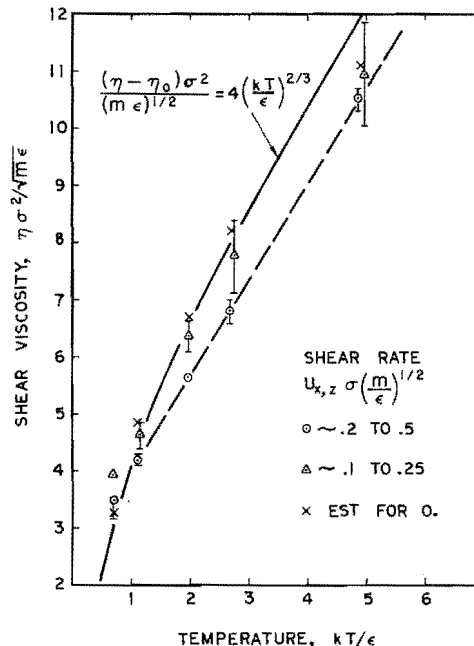


FIG. 10. Lennard-Jones shear viscosity along the freezing line. Calculated with 108 atoms at two shear rates (see Table VII). The lowest x is the estimated infinite-width triple-point value (see Table VI). The dashed line indicates the large-shear-rate linear temperature dependence, while the solid line is a nonlinear fit in terms of the inverse-12th-power scaling variables.

dependence, they obtain an approximation for the freezing-line shear viscosity

$$\eta\sigma^2/(m\epsilon)^{1/2} \approx 5(kT/\epsilon)^{0.63}.$$

They do not comment on the power dependence of temperature and its relation to the inverse-power scaling. Since the viscosity increases with temperature along the freezing line (similar to dilute gases) but decreases with increasing temperature along the saturated-vapor-pressure line, there must be a transition region. Sengers⁴ discusses this general phenomenon of the change of slope of viscosity isotherms when plotted against pressure or density—i.e., $(\partial\eta/\partial T)_p$ changes sign. Experimentally these isotherms intersect at about twice the critical density, while calculations for the isotherms of $kT/\epsilon = 8.5$ and 28 indicate an intersection at three times the critical density (see following).

D. Density and temperature dependence of the Lennard-Jones excess shear viscosity

Although pressure is a more convenient experimental variable, the isothermal density dependence of the shear viscosity and thermal conductivity is simpler to describe. The dilute-gas (zero-density limit) temperature dependence is well described by kinetic theory. Experiment suggests that the excess shear viscosity $\Delta\eta$ [$\equiv(\eta - \eta_0)$, where η_0 is the dilute-gas value] is almost temperature independent. While Andrade's simple paradigm for shear viscosity has no temperature dependence, the Enskog hard-sphere theory produces a square-root temperature dependence. However, the experimental shear viscosity of argon, hydrogen, helium, oxygen, and carbon dioxide indicates a weak temperature dependence with a negative temperature derivative (at constant density). The excess thermal conductivity (with the exception of the critical region) has behavior similar to that of shear viscosity, except that the experimental data indicate a positive rather than a negative isochoric temperature derivative.^{44,47}

Diller⁴⁸ was able to represent his experimental shear viscosity for para-hydrogen at cryogenic temperatures ($<100^\circ\text{K}$) and for densities up to ~800 amagats with an empirical equation of the form

$$\eta = \eta_0(T) + A(\rho)e^{B(\rho)/T},$$

where $\eta_0(T)$ is the low-density viscosity, and A and B are complicated functions determined from his experimental data. These same density coefficients also correlate (within 3%) with Michels *et al.*⁴⁹ experimental shear-viscosity data for normal hydrogen at room temperature (density up

to 800 amagats). For thermal conductivity, both Rosenbaum *et al.*⁵⁰ and Bailey and Kellner⁵¹ found that their experimental argon data could be reproduced (to within 3%) by the empirical relation

$$\lambda = \lambda_0(T) + A(e^{B\rho} - 1)$$

(temperature range $90-350^\circ\text{K}$, pressures up to 1000 atm). Thus the excess coefficients appear to be valuable density-scaling functions. Therefore, to investigate this phenomenon, the Lennard-Jones shear viscosity has been calculated for two isotherms corresponding to room temperature for hydrogen and helium ($kT/\epsilon = 8.5$ and 28).

The nonequilibrium molecular-dynamic calculations used 108 Lennard-Jones atoms in a unit cube (Table VIII). A few calculations were also made with 216 particles (two 108-cubes wide), and these results indicate only a slight increase in shear viscosity compared to the 108-particle results. The calculations are done at fixed density, but the momentum flux (pressure) and temperature are determined from finite-time averages and thus have some uncertainty. The compressibility factors from these runs agree well with Hansen's Lennard-Jones equation of state.²² For densities near and below critical density (0.36 for Lennard-Jones, for hydrogen about 520 amagats), the Enskog estimate is in reasonable agreement with the molecular-dynamic results. For larger densities, the deviation of Enskog estimates from the molecular-dynamic results grows to about a factor of 2 near the freezing density (~1.5). This disagreement is similar to that found by Alder, Gass, and Wainwright in their equilibrium molecular-dynamic studies of the hard-sphere system. The Enskog estimate indicates a positive value for $\partial\Delta\eta/\partial T$, the opposite of experimental observation and the molecular-dynamic results.

Figure 11 shows that the calculated reduced excess shear viscosity for both of these isotherms can be correlated with the soft-sphere scaling variables,

$$\Delta\eta\sigma^2(m\epsilon)^{-1/2}(\epsilon/kT)^{2/3} = 7.07x^4. \quad (1)$$

This fit clearly reveals two features: (i) weak temperature dependence and (ii) a negative temperature derivative at constant density $d\ln\Delta\eta/d\ln T = -\frac{1}{3}$. Notice that the temperature derivative is negative for any power of x greater than $\frac{8}{3}$. While both of these features have been experimentally observed in simple-fluid shear-viscosity data (e.g., argon, helium, hydrogen, oxygen, and carbon dioxide; see Refs. 44 and 47), their cause has not been previously traced to the dominance of the core potential. For all x , a slightly better fit is given by the empirical relation

$$\Delta\eta\sigma^2(m\epsilon)^{-1/2}(\epsilon/kT)^{2/3} = 0.024(e^{6x} - 1) \quad (2)$$

(dashed line in Fig. 11). Note that the temperature derivative is *positive* for low-density-high-temperature combinations and only becomes negative for x greater than 0.41.

The soft-sphere shear viscosity alone can be fitted ($\sim 3\%$ error) by the empirical relation

$$\Delta\eta\sigma^2(m\epsilon)^{-1/2}(\epsilon/kT)^{2/3} = 0.0152(e^{7.02x} - 1), \quad (3)$$

where the product of the coefficients was required to equal the soft-sphere Enskog first density correction to the dilute-gas shear viscosity [0.107—see Eq. (26) of Ref. 44]. For x less than 0.5, the Enskog theory provides a good soft-sphere shear viscosity estimate; however, for higher densities, the molecular-dynamic results are 2 to 3 times the Enskog values.

There is a small discrepancy in the coefficient values of Eqs. (2) and (3), which at infinite temperature must be equivalent. Procrustean fitting [guided by the inverse square-root temperature expansion of the second and third Lennard-Jones virial coefficients (see p. 1119 of Ref. 1), since they determine the Enskog first density correction] of all the nonequilibrium molecular-dynamic results yields the empirical relation

$$\begin{aligned} &\Delta\eta\sigma^2(m\epsilon)^{-1/2}(\epsilon/kT)^{2/3} \\ &= 0.0152[1 - 0.5(\epsilon/kT)^{1/2} + 2.0(\epsilon/kT)] \\ &\times (\exp\{7.02x[1 - 0.2(\epsilon/kT)^{1/2}]\} - 1), \end{aligned}$$

with a fit error of 5–10% of the excess or dilute shear viscosity (whichever is larger). Thus the utilization of the soft-sphere scaling variables yields a relatively simple function describing the excess Lennard-Jones shear viscosity throughout the fluid phase. The experimental argon shear-viscosity data of Michels *et al.*⁵¹ and Haynes⁴⁶ spans the density range from dilute gas to saturated liquid; however, compared to the molecular-dynamic conditions the reduced temperature variation is small (0.7–2.9). Fitting the data using the soft-sphere scaling variables yields

$$\Delta\eta\sigma^2(m\epsilon)^{-1/2}(\epsilon/kT)^{2/3} = 0.0324(e^{5.18x} - 1).$$

Comparison with a fit of $\Delta\eta$ versus density ρ (with the same function) indicates reduction of the relative fit error by factors of 7 (for high ρ and T) to 3 (for high ρ and low T) and thus confirms the value of the inverse-power scaling variables. Therefore this new way of scaling excess shear viscosity should be useful for empirical correla-

TABLE VIII. Nonequilibrium molecular-dynamic 108-atom results for Lennard-Jones shear viscosity as a function of density along the isotherms $kT/\epsilon = 8.5$ and 28, (dilute-gas shear viscosity is 0.61 and 1.32). Four-run average; see Table I caption (* $N = 216$, $kT_0/\epsilon = 9.2$ and 30). Zero-shear-rate estimate marked by **. Compressibility factor from velocity zone momentum flux and L-J equation of state (Ref. 22). Thermal conductivity estimated from zone temperature distribution.

$N\sigma^3/V$	kT/ϵ	$u_{x,z}\sigma\left(\frac{m}{\epsilon}\right)^{1/2}$	$\eta\sigma^2(m\epsilon)^{-1/2}$	PV/NkT		$\lambda\sigma^2(m/\epsilon)^{1/2}/k$	
				Calculated	EOS	Estimated	Enskog
0.25	8.41	0.20	0.61 ± 0.08	1.35	1.34	2.1 ± 1.6	3.04
0.35	8.58	0.32	0.74 ± 0.06	1.58	1.55	$3.49 (\pm ?)$	3.57
0.40	8.58	0.34	0.94 ± 0.09	1.71	1.67		3.88
0.50	8.48	0.36	1.00 ± 0.03			1.98	4.62
0.55	8.63	0.37	1.28 ± 0.11	2.25	2.18	$2.67 (\pm ?)$	5.11
0.60	8.51	0.50	1.24 ± 0.12	2.48	2.40	11.1 ± 3	5.60
0.80	8.56	0.56	2.16 ± 0.07	3.74	3.63	$8.0 (\pm ?)$	8.35
1.00	9.12	0.15	3.29 ± 0.17	5.65	5.57		12.6
1.20	8.72	0.68	6.45 ± 0.16	8.75	8.76	20.4 ± 2	18.0
	9.09	0.16	7.83 ± 0.30	8.58	8.62		
	9.09	$\sim 0^{**}$	8.26 ± 0.30				
1.40	8.85	0.71	12.60 ± 0.31	13.03	13.68	31.8 ± 4	24.8
	9.11	0.19	13.97 ± 1.1	12.87	13.2		
	9.10	0.19	$13.41 \pm 0.63^*$	12.85	13.2	19.3 ± 5	25.2
		$\sim 0^{**}$	13.62 ± 0.63				
0.25	28.67	0.35	1.19 ± 0.24	1.35	1.35		6.3
0.55	27.97	0.75	1.71 ± 0.08	2.06	2.04		8.91
0.80	27.59	0.94	2.85 ± 0.30	3.03	3.00	12.1 ± 8	12.7
1.2	28.30	1.25	5.77 ± 0.36	5.65	5.66	17.5 ± 10	23.2
1.4	27.86	1.24	9.46 ± 0.30	7.77	7.85	36.8 ± 15	30.9
	29.70	0.35	$9.95 \pm 0.40^*$	7.55		17.8 ± 8	

tions of experimental data over the complete fluid range.

V. CONCLUSION

The method of nonequilibrium molecular dynamics has been developed to simulate dense-fluid transport of momentum and energy. This new method also allows determination of nonequilibrium distribution functions which should provide the basis for a perturbation theory of transport. Shear viscosity of soft spheres (r^{-12} potential) and Lennard-Jones particles ($r^{-12}-r^{-6}$ potential) has been obtained from molecular-dynamic modeling of Couette flow. Soft-sphere deviations from Enskog theory are similar to those found for hard spheres by Alder, Gass, and Wainwright, using time correlations of equilibrium molecular-dynamic system fluctuations. For densities near freezing, the nonequilibrium calculations have a non-Newtonian behavior; however, the Ree-Eyring inverse-hyperbolic-sine shear-rate dependence gives an excellent portrayal of the calculated results and has been used to estimate the zero-shear-rate shear viscosity. For the Lennard-Jones shear viscosity near the triple-point region, there is

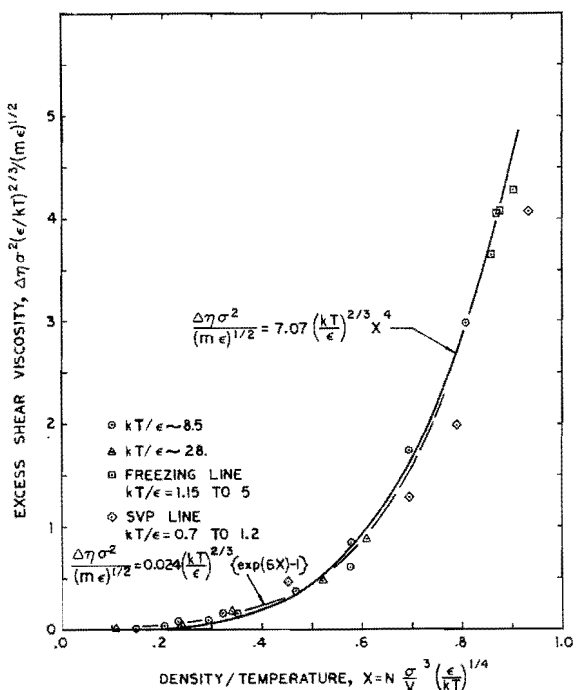


FIG. 11. Calculated Lennard-Jones excess shear viscosity along the isotherms $kT/\epsilon \approx 8.5$ and 28 expressed in terms of the single repulsive 12th-power scaling variables. Also shown, but not used in determining the curve fits, are calculated Lennard-Jones shear viscosities along the (L-J) freezing line and the saturated-vapor-pressure line (of argon).

agreement between the equilibrium result of Levesque, Verlet, and Kurkijarvi and the nonequilibrium zero shear-rate using 108 atoms in a cube. However, systems two and three cubes wide yield lower results, which, when extrapolated with inverse width, are in close agreement with the experimental argon shear viscosity. This same size dependence is in qualitative agreement with hydrodynamic experiments on spheres moving in a viscous fluid and is also supported by the mathematical analogy between elastic solids and viscous liquids. The triple-point equilibrium viscosity results can also be brought into agreement with both the nonequilibrium and experimental viscosities if a similar inverse width correction applies to that method. The equilibrium result for the Lennard-Jones thermal conductivity is twice the experimental argon value and the nonequilibrium results (which appear to have weak dependence upon system size and temperature gradient). Comparison of the Lennard-Jones shear viscosity with experimental argon data along the saturated-vapor-pressure line of argon confirms our successful simulation of macroscopic viscous flow with few-particle nonequilibrium molecular-dynamic systems.

The soft-sphere system, being a single inverse-nth-power potential, has a special scaling feature; reduced viscosity and thermal conductivity times $(\epsilon/kT)^{1/2+2/n}$ are universal functions of the reduced density times $(\epsilon/kT)^{1/n}$ throughout the fluid phase. Since momentum transport is primarily accomplished by the repulsive potential core for high temperatures, the Lennard-Jones shear viscosity must behave like the soft-sphere system for high temperatures. In fact, the calculated excess shear viscosity (that part above the zero-density temperature dependence) has been successfully correlated in terms of the 12th-power scaling variables for temperatures as low as the critical value (along the freezing line). The molecular-dynamic results for thermal conductivity differ from shear viscosity in that the equilibrium calculations for hard-spheres (done by Alder, Gass, and Wainwright) and the nonequilibrium calculations¹⁵ for soft spheres and Lennard-Jones potential are in reasonable agreement with their respective Enskog estimates over the complete fluid-density range (and even into the solid region for hard spheres). Calculated freezing-line Lennard-Jones thermal conductivities have the soft-sphere temperature dependence $(kT/\epsilon)^{2/3}$ and lie only 30% above the Enskog estimate. The calculated Lennard-Jones excess thermal-conductivity coefficient agrees with the experimental argon density dependence. The utilization of the soft-sphere scaling variables yields relatively

simple functions for describing the excess shear viscosity and thermal-conductivity behavior throughout the fluid phase. The introduction of these scaling variables also clearly reveals two features: (i) weak temperature dependence and (ii) the sign of the temperature derivative at constant density (negative for shear viscosity and positive for thermal conductivity). While both of

these features have been experimentally observed in simple-fluid experimental data (e.g., argon, helium, hydrogen, oxygen, and carbon dioxide), their cause has not been previously traced to the dominance of the core potential. Thus the soft-sphere scaling variables should be useful for correlating experimental data.

*Work performed under the auspices of the U.S. Atomic Energy Commission.

[†]Work done in partial fulfillment of the requirements for a Ph.D., University of California at Davis, Department of Applied Science, at Livermore.

[‡]J. O. Hirschfelder, C. F. Curtiss, and R. B. Bird, *Molecular Theory of Gases and Liquids* (Wiley, New York, 1964), Chaps. 7, 9, and 11.

[§]J. A. Barker, M. V. Bobetic, and A. Pompe, *Mol. Phys.* 20, 347 (1971).

[¶]Reference 1, p. 649.

[¶]J. V. Sengers, *Recent Adv. Eng. Sci.* 3, 153 (1966); J. V. Sengers, *Int. J. Heat Mass Transfer* 8, 1103 (1965).

[¶]H. N. V. Temperley, J. S. Rowlinson, and G. S. Rushbrooke, *Physics of Simple Liquids* (Wiley, New York, 1968), Chaps. 4 and 5.

[¶]B. J. Alder and T. E. Wainwright, *J. Chem. Phys.* 31, 459 (1959); 33, 1439 (1960).

[¶]M. S. Green, *J. Chem. Phys.* 20, 1281 (1952); 22, 398 (1954); R. Kubo, *J. Phys. Soc. Jpn.* 12, 570 (1957); R. Kubo, M. Yokota, and S. Nakajima, *J. Phys. Soc. Jpn.* 12, 1203; E. Helfand, *Phys. Rev.* 119, 1 (1960); R. Zwanzig, *Ann. Rev. Phys. Chem.* 16, 67 (1965); D. Gass, *J. Chem. Phys.* 51, 4560 (1969); S. G. Brush, *Kinetic Theory* (Pergamon, New York, 1972), Vol. 3, pp. 69-72.

[¶]B. J. Alder, D. M. Gass, and T. E. Wainwright, *J. Chem. Phys.* 53, 3813 (1970).

[¶]W. M. Visscher, *Phys. Rev. A* 7, 1439 (1973).

[¶]A. Rahman, *Phys. Rev.* 136, A405 (1964).

[¶]L. Verlet, *Phys. Rev.* 159, 98 (1967); 165, 201 (1968); D. Levesque and L. Verlet, *Phys. Rev. A* 2, 2514 (1970).

[¶]C. Bruin, *Phys. Lett.* 28A, 777 (1969).

[¶]A. N. Lagar'kov and V. M. Sergeev, *Teplofiz. Vys. Temp.* 8, 1309 (1970) [High Temp. 8, 1232 (1970)].

[¶]E. M. Gosling, I. R. McDonald and K. Singer, *Mol. Phys.* 26, 1475 (1973).

[¶]W. T. Ashurst, Ph.D. dissertation (University of California, 1974) (unpublished). Some preliminary results were given in *Phys. Rev. Lett.* 31, 206 (1973) by W. T. Ashurst and W. G. Hoover. For the long-time behavior of the velocity autocorrelation see D. Levesque and W. T. Ashurst, *Phys. Rev. Lett.* 33, 277 (1974).

[¶]W. G. Hoover, M. Ross, K. W. Johnson, D. Henderson, J. A. Barker, and B. C. Brown, *J. Chem. Phys.* 52, 4931 (1970).

[¶]W. G. Hoover, S. G. Gray, and K. W. Johnson, *J. Chem. Phys.* 55, 1128 (1971). H. Matsuda and Y. Hiwatari, in *Cooperative Phenomena*, edited by H. Haken and M. Wagner (Springer, Berlin, 1973), p. 250.

[¶]L. Verlet and J. J. Weis, *Phys. Rev. A* 5, 939 (1972).

[¶]H. Schlichting, *Boundary Layer Theory*, 4th ed. (McGraw-Hill, New York, 1960), pp. 66, 306, and 491.

[¶]H. W. Liepmann and A. Roshko, *Elements of Gasdynamics* (Wiley, New York, 1957).

[¶]We thank F. Ree for calling Eyring's work to our attention. See for instance, F. H. Ree, T. Ree, and H. Eyring, *Ind. Eng. Chem.* 50, 1036 (1958); H. Eyring, D. Henderson, B. J. Stover, and E. M. Eyring, *Statistical Mechanics and Dynamics* (Wiley, New York, 1964), p. 462.

[¶]J. P. Hansen, *Phys. Rev. A* 2, 221 (1970).

[¶]E. N. Da C. Andrade, *Philos. Mag.* 17, 497 (1934); 17, 698 (1934); *Viscosity and Plasticity* (Chemical, New York, 1951).

[¶]E. McLaughlin, *Chem. Rev.* 64, 389 (1964).

[¶]H. Lamb, *Hydrodynamics* (Dover, New York, 1945).

[¶]R. Zwanzig and M. Bixon, *Phys. Rev. A* 2, 2005 (1970); see also A. F. Collings, *Am. Inst. Chem. Eng. J.* 19, 183 (1973); L. A. Woolf, *J. Chem. Phys.* 57, 3013 (1972).

[¶]M. Ross and P. Schofield, *J. Phys. C* 4, L305 (1971).

[¶]Y. Hiwatari, H. Matsuda, T. Ogwa, N. Ogita, and A. Uda, *Prog. Theor. Phys.* (to be published).

[¶]K. D. Timmerhaus and H. G. Drickamer, *J. Chem. Phys.* 20, 981 (1952).

[¶]J. A. Pryde, *The Liquid State* (Hutchinson, London, 1966), Chap. 9.

[¶]H. S. Green, in *Encyclopedia of Physics*, edited by S. Flügge (Springer, Berlin, 1960), Vol. 10. Green assumes $\nu(r)$ to be a constant over the range of interest and hence removes it from the integral (p. 110). Another approach has tried to combine three-particle and higher correlations from equilibrium systems to approximate $\nu(r)$. See I. Prigogine, G. Nicolis and J. Misguich, *J. Chem. Phys.* 43, 4516 (1965), and references therein. The Rice theory has since been disproven by R. A. Fisher and R. O. Watts [Aust. J. Phys. 25, 21 (1972)] and A. F. Collings, R. O. Watts, and L. A. Woolf [Mol. Phys. 20, 1121 (1971)]. These approximations have provided results which differ from argon data by factors of 2. See J. A. Palyvos *et al.*, *J. Chem. Phys.* 49, 4088 (1968).

[¶]J. I. Frenkel, *Kinetic Theory of Liquids* (Dover, New York, 1955).

[¶]T. W. Chapman, *Am. Inst. Chem. Eng. J.* 12, 395 (1966). This work presents an erroneous form for $\nu(r)$, but utilizes the concept of an integral of an unknown function to obtain a corresponding states scaling for liquid-metal viscosity. For a correlation of viscosity and self-diffusion of 10 liquid metals see A. D. Pasternak, *Phys. Chem. Liquids* 3, 41 (1972).

- ³⁴W. G. Hoover, A. C. Holt, and D. R. Squire, *Physica* (Utr.) 44, 437 (1969); D. R. Squire, A. C. Holt, and W. G. Hoover, *Physica* (Utr.) 42, 388 (1969).
- ³⁵R. Zwanzig and R. D. Mountain, *J. Chem. Phys.* 43, 4464 (1965); R. D. Mountain and R. Zwanzig, *J. Chem. Phys.* 44, 2777 (1966).
- ³⁶D. Levesque, L. Verlet, and J. Kurkijarvi, *Phys. Rev. A* 7, 1690 (1973).
- ³⁷J. Hansen and L. Verlet, *Phys. Rev.* 184, 151 (1969); J. A. Barker, R. A. Fisher, and R. O. Watts, *Mol. Phys.* 21, 657 (1971).
- ³⁸J. P. Boon, J. C. Legross, and G. Thomaes, *Physica* (Utr.) 33, 547 (1967).
- ³⁹H. Ziebland and J. T. A. Burton, *Brit. J. Appl. Phys.* 9, 52 (1958); A. Uhlig, *J. Chem. Phys.* 20, 463 (1952); B. J. Bailey and K. Kellner, *Physica* (Utr.) 39, 444 (1968).
- ⁴⁰J. Hellemans, H. Zink, and O. van Paemel, *Physica* (Utr.) 46, 395 (1970).
- ⁴¹W. G. Hoover, W. T. Ashurst, and R. J. Olness, *J. Chem. Phys.* 60, 4043 (1974).
- ⁴²J. R. Partington, *An Advanced Treatise on Physical Chemistry, Volume 2, The Properties of Liquids* (Longmans, Green, London, 1955), pp. 86-87.
- ⁴³D. Levesque and L. Verlet, *Phys. Rev.* 182, 307 (1969); see also P. D. Neufeld, A. R. Janyen, and R. A. Aziz, *J. Chem. Phys.* 57, 1100 (1972). Note that they did not force their empirical fit of $\Omega^{(2,2)}$ to have the known high-temperature limit (i.e., soft-sphere $1.296/T^{*1/6}$).
- ⁴⁴H. J. M. Hanley, R. D. McCarty, and E. G. D. Cohen, *Physica* (Utr.) 60, 322 (1972).
- ⁴⁵A. De Bock, W. Grevendonk, and W. Herremans, *Physica* (Utr.) 37, 227 (1967).
- ⁴⁶W. M. Haynes, *Physica* (Utr.) 67, 440 (1973).
- ⁴⁷D. E. Diller, H. J. M. Hanley, and H. M. Roder, *Cryogenics* 10, 286 (1970).
- ⁴⁸D. E. Diller, *J. Chem. Phys.* 42, 2089 (1965).
- ⁴⁹A. Michels, A. C. J. Schipper, and W. H. Rintoul, *Physica* (Utr.) 19, 1011 (1953).
- ⁵⁰B. M. Rosenbaum, S. Oshen, and G. Thodos, *J. Chem. Phys.* 44, 2831 (1966).
- ⁵¹A. Michels, J. V. Sengers, and L. J. M. Van De Klundert, *Physica* (Utr.) 29, 149 (1963).